AN INVESTIGATION OF MOMENTUM EXCHANGE PARAMETERIZATIONS AND ATMOSPHERIC FORCING FOR THE COASTAL MIXING AND OPTICS PROGRAM

by

Michiko J. Martin

M.S., Troy State University (1996)
B.S., United States Naval Academy (1991)

MASSACHUSETTS INSTITUTE OF TECHNOLOGY
JUN 21 1999
LIBRARIES
Eng.

Submitted in partial fulfillment of the
requirements for the degree of

MASTER OF SCIENCE
at the
MASSACHUSETTS INSTITUTE OF TECHNOLOGY
and the
WOODS HOLE OCEANOGRAPHIC INSTITUTION

September 1998

© Michiko J. Martin, 1998. All rights reserved.
The author hereby grants to MIT, WHOI, and the United States Navy permission to reproduce and to distribute copies of this thesis document in whole or in part.

Signature of Author.....
Joint Program in Applied Ocean Physics and Engineering
Massachusetts Institute of Technology and Woods Hole Oceanographic Institution

Certified by .....
James B. Edson
Associate Scientist, Woods Hole Oceanographic Institution
Thesis Supervisor

Certified by .....
Steven P. Anderson
Associate Scientist, Woods Hole Oceanographic Institution
Thesis Reader

Approved by .....
Michael S. Triantafyllou
Chairman, Joint Committee for Applied Ocean Physics and Engineering
Massachusetts Institute of Technology and Woods Hole Oceanographic Institution

AN INVESTIGATION OF MOMENTUM EXCHANGE PARAMETERIZATIONS

AND ATMOSPHERIC FORCING FOR THE COASTAL MIXING AND OPTICS PROGRAM

by

Michiko J. Martin

Submitted in partial fulfillment of the requirements for the degree of
Master of Science at the Massachusetts Institute of Technology and the
Woods Hole Oceanographic Institution.

September 1998

ABSTRACT

This thesis presents an investigation of the influence of surface waves on momentum exchange. A quantitative comparison of direct covariance friction velocity measurements to bulk aerodynamic and inertial dissipation estimates indicates that both indirect methods systematically underestimate the momentum flux into developing seas. To account for wave-induced processes and yield improved flux estimates, modifications to the traditional flux parameterizations are explored.

Modification to the bulk aerodynamic method involves incorporating sea state dependence into the roughness length calculation. For the inertial dissipation method, a new parameterization for the dimensionless dissipation rate is proposed. The modifications lead to improved momentum flux estimates for both methods.

Thesis Supervisor: Dr. James B. Edson
Title: Associate Scientist, Woods Hole Oceanographic Institution

ACKNOWLEDGMENTS

I would like to express my sincere thanks to my advisor Dr. Jim Edson. His motivation and enthusiasm are inspiring, and his dedication to science and research is matched by his ability and patience to teach.

I would also like to thank Dr. Steve Anderson for his support throughout this project and his help as a reader of this thesis.

I am also grateful to the staff and faculty of the Ocean Engineering Department at MIT and the Applied Ocean Physics and Engineering, Education, and Physical Oceanography Departments at WHOI, particularly Jean Sucharewicz, Julia Westwater, and Drs. Mark Grosenbaugh, Al Plueddemann, Steve Lentz and Mark Baumgartner.

The love, warmth, and support of my family have sustained and stimulated me. This is dedicated to my parents for their continual support, encouragement, and confidence.

This project was funded by the Oceanographer of the Navy.

TABLE OF CONTENTS

1. INTRODUCTION

2. EXPERIMENT
   2.1. DEPLOYMENT AND SITE SELECTION
   2.2. CMO INSTRUMENTATION AND DATA PROCESSING
      2.2.1. VECTOR AVERAGING WIND RECORDER
      2.2.2. SONIC ANEMOMETER
      2.2.3. WAVE HEIGHT MEASUREMENTS
   2.3. MARINE BOUNDARY LAYER EXPERIMENT

3. THEORY
   3.1. BASIC EQUATIONS
   3.2. EQUATIONS FOR TURBULENT MEAN FLOW
   3.3. EQUATIONS FOR TURBULENT KINETIC ENERGY

4. METHODOLOGY
   4.1. DIRECT TECHNIQUES TO DETERMINE THE MOMENTUM FLUX
      4.1.1. DIRECT COVARIANCE (EDDY CORRELATION) METHOD
      4.1.2. MOTION-CORRECTED COVARIANCE METHOD
   4.2. INDIRECT TECHNIQUES TO DETERMINE THE MOMENTUM FLUX
      4.2.1. MEAN PROFILE METHOD
      4.2.2. BULK AERODYNAMIC METHOD
      4.2.3. DIRECET AND INERTIAL DISSIPATION METHODS

5. ANALYSIS AND RESULTS
   5.1. DATA SELECTION
   5.2. TRADITIONAL APPROACH
   5.3. MODIFIED INERTIAL DISSIPATION METHOD
   5.4. MODIFIED BULK AERODYNAMIC METHOD
      5.4.1. SCALING ROUGHNESS LENGTH WITH WAVE AMPLITUDE
      5.4.2. MODIFIED CHARNOCK'S RELATION

6. CONCLUSIONS

1. INTRODUCTION

Successful investigations of air-sea interactions across the ocean surface depend on accurate measurements of the exchange of momentum and energy between the air and ocean. The exchange of heat energy between the atmosphere and the ocean is driven by molecular, turbulent, and radiative processes and is given by the surface heat budget

$$Q_{SEA} = Q^* - Q_H - Q_E \tag{1.1}$$

where Q_{SEA} is the net heat input into the ocean; Q^* represents the net downward radiation (irradiance); and, Q_H and Q_E are the upward fluxes of sensible and latent heat, respectively. The radiative processes at the surface can be further expressed as

$$Q^* = SW - LW \tag{1.2}$$

where the net irradiance Q^* results from the absorption of solar (shortwave) radiation SW less the loss to the atmosphere through net infrared (longwave) radiative transfer LW (Bradley *et al.*, 1991). The radiative forcing of the atmosphere produces temperature and pressure gradients that result in the generation of winds of the order of 10 ms^{-1} and is responsible for large-scale atmospheric circulations.

The exchange of sensible Q_H and latent Q_E heat occur as a result of conduction, turbulence, and convection. Conduction is important only within the molecular sublayer, within approximately 1 millimeter of the ocean's surface, where fluid motions are strongly suppressed by viscosity. Immediately above the molecular boundary layer but below the mixed layer, which is characterized by deep convection and thermally-driven circulations, is the near-surface layer for which microscale turbulence due to shear is the dominant type of fluid motion. Sensible heat and water vapor are transferred via

microscale eddies, which are induced mechanically by flow over irregularities in the surface (Wallace and Hobbs, 1977), and larger eddies which feed off the mean wind shear (velocity gradient). Above this shear layer, turbulent eddies are generated by a combination of shear and buoyancy. In turn, these turbulent eddies modify the instantaneous shear and give winds their "gusty" nature by transferring momentum by bodily movement of air parcels, *i.e.*, by fast-moving parcels moving downward and slow-moving parcels moving upward (Gill, 1982). Since momentum is mass times velocity, its transfer per unit area per unit time can be expressed as a flux $\widetilde{F}$ which has the SI units $\frac{\mathrm{kg}\left(\mathrm{ms}^{-1}\right)}{\mathrm{m}^2\mathrm{s}}$, which is identical to $\frac{\mathrm{N}}{\mathrm{m}^2}$, the units for stress. This transfer of momentum, or shear stress, from the winds to the ocean drives the waves and wind-driven ocean currents and provides kinetic energy for mixing in the ocean mixed layer.

Together with radiative transfer, the exchange of sensible and latent heat are important mechanisms for redistributing energy between the atmosphere and ocean. An understanding of the dynamics and magnitude of this energy transfer is required for the initialization and excursion of coupled air-ocean models. Even the most crude global circulation models must place a lower boundary condition on the mean atmospheric variables and fluxes. With ever growing computational power and sophistication of numerical models, the importance of incorporating a realistic atmospheric boundary layer increases tremendously. Current research (*e.g.*, Webster and Lukas, 1992; Miller *et al.*, 1992) continues to demonstrate that more accurate parameterization of these fluxes directly leads to improved model simulations. Whereas an additional input of only 10 Wm^{-2} to the ocean and troposphere has significant climatological effects, the

uncertainty in current estimates of the surface heat budget exceeds this value, with discrepancies as large as 80 Wm^{-2} in the warm pool region of the western Pacific Ocean (Bradley *et al.*, 1991). Decreasing this uncertainty and providing improved estimates of the heat budget will result in increased performance in numerical models and improve our ability to diagnose and predict climate and climate variability.

The research presented in this thesis is an investigation of the influence of wave-induced processes on momentum exchange. The thesis explores modifications to traditional flux parameterizations to account for sea state. This is accomplished by investigating two separate approaches to incorporate sea state dependence into the roughness length determination in the bulk aerodynamic method and a new approach to incorporate wave-induced effects in the dimensionless dissipation rate in the inertial dissipation method. Both investigations rely on comparison of the parameterized fluxes with direct covariance fluxes.

Details of the experiment, instrumentation, and data processing are described in Chapter 2. Chapters 3 and 4 provide the theoretical framework upon which this investigation is based. A detailed derivation of the turbulent kinetic energy budget is presented in Chapter 3, and a summary of the four standard techniques for estimating the momentum flux, including an introduction to the well-accepted Monin-Obukhov similarity theory, is provided in Chapter 4. Alternate parameterizations for both the bulk aerodynamic and inertial dissipation methods are presented in Chapter 5, and their performance is evaluated. The final chapter summarizes the findings of this thesis and suggests areas of future research.

2. EXPERIMENT

2.1. DEPLOYMENT AND SITE SELECTION

The data used in this investigation were collected during the Coastal Mixing and Optics (CMO) experiment, an Accelerated Research Initiative supported by the Office of Naval Research (Williams, 1997; Galbraith *et al.*, 1997). Four moorings were deployed from August 1996 to June 1997 in the Middle Atlantic Bight, 90 km south of Martha's Vineyard at approximately 40.5°N, 70.5°E, as depicted in Figure 2.1. The four moorings included a central mooring on the 70 m isobath, an inshore mooring located approximately 10 km inshore along the 60 m isobath, an offshore mooring located 10 km offshore along the 80 m isobath, and an alongshore mooring located 25 km east of the central buoy along the 70 m isobath. The region has fine sediment and a smooth bottom that slopes gently towards the shelf break 40 km to the south. The large-scale surface heating and buoyancy advection at this site create a strong thermocline/pycnocline during the late-spring and summer months. The extensive deployment was chosen so that the observation period included the destruction of thermal stratification of the water column in the fall and the subsequent redevelopment of stratification in the spring. In addition to recording the seasonal evolution of stratification, the passage of numerous frontal systems as well as the transits of Hurricanes Edouard and Hortense were observed. Due to the variety of weather phenomena experienced at the site during the eleven-month deployment, this data set represents a wide range of conditions and is unequaled in previous investigations of mixing processes in coastal/shelf waters.

2.2. Coastal Mixing and Optics (CMO) Instrumentation and Data Processing

While all moorings were outfitted with environmental sensors, the data used in this study was obtained from the instrumentation on board the CMO central discus. The central three-meter buoy, shown in Figure 2.2, supported sensors to measure a variety of oceanic and atmospheric properties. The buoy had a draft of about 1.5 m and extended approximately 3.5 m above the water line. The buoy was outfitted with a large steering vane mounted to one of the mast legs that served to minimize flow distortion by generally providing the best exposure of the meteorological instruments.

2.2.1. Vector Averaging Wind Recorder

The central buoy carried two, redundant Vector Averaging Wind Recorder (VAWR) meteorological packets (Weller *et al.*, 1990). The VAWR sensors measured wind speed and direction, air and sea surface temperatures, barometric pressure, relative humidity, and incoming short-wave and long-wave radiation at a 15-minute sampling rate (Baumgartner and Anderson, 1997). The sensor specifications for the VAWR meteorological package are listed in Table 1.

Table 1. VAWR sensor specifications. Wind speed and direction are vector averaged over the sampling interval. Heights are reported as meters above the mean water line. [From Baumgartner and Anderson, 1997 (Table 5).]

Parameter	Sampling Interval	Range	Accuracy	Height
Wind speed	15 minute average	0.2-50.0 ms^{-1}	±2% above 0.7 ms^{-1}	3.30
Wind direction	15 minute average	0-360°	±5.6°	3.02
Air temperature	3.75 minute average	-10-35 °C	±0.2 °C when wind > 5 ms^{-1}	2.63
Sea temperature	3.75 minute average	-5-30 °C	±0.005 °C	-1.46
Barometric pressure	2.5 second sample	0-1034 mbar	±0.2 mbar when wind < 20 ms^{-1}	2.72
Relative humidity	3.5 second sample	0-100%	±2%	2.68
Short-wave radiation	15 minute average	0-140 W m^{-2}	±3% of value	3.39
Long-wave radiation	15 minute average	0-700 W m^{-2}	±10%	3.40

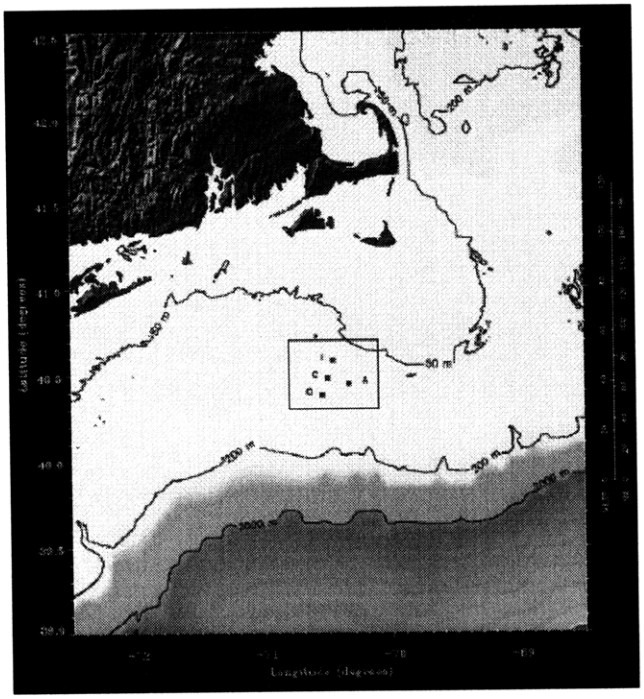

Figure 2.1. Coastal Mixing and Optics Site. [From Stenner, 1996.]

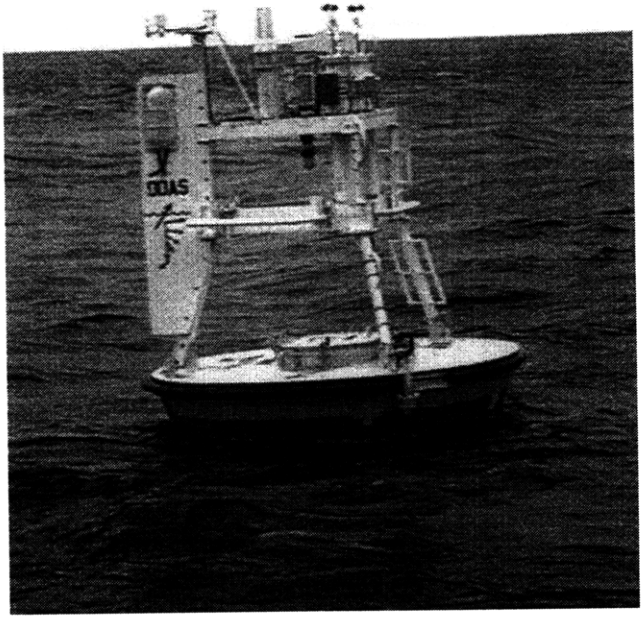

Figure 2.2. Coastal Mixing and Optics central 3 m discus buoy. [From Baumgartner and Anderson, 1997 (Figure 4).]

2.2.2. SONIC ANEMOMETER

The central buoy also held a sonic anemometer which measured the longitudinal, lateral and vertical wind velocities as well as the speed of sound. The sonic was mounted between the VAWR wind sensors at a height 3.3 m above the sea surface and was configured to burst sample twice per hour for a duration of 15 minutes.

Manufactured by Gill Instruments Ltd., the sonic consists of a sensing head and three ultrasonic transducer pairs supported by three struts. The struts are placed asymmetrically to provide $\pm 120°$ of open exposure. The sonic anemometer is specified to operate with 1.5% accuracy for wind speeds between 0-60 ms^{-1} (Yelland *et al.*, 1994). Each pair of transducers alternately transmits and receives pulses of high frequency sound waves. All three axes complete these firings every 6 ms, which represents a sampling rate of 168 Hz. Using overlap section averaging, every eight complete transit time evaluations are averaged to produce the 21 Hz output. The transit time data were transformed into an orthogonal coordinate system by which the speed of sound and wind velocity were calculated by determining the times of flight, t_1 and t_2, between any pair of transducers. Specifying V as the air flow parallel to the line of the transducer pair, the flight times are defined by

$$t_1 = \frac{l}{c+V} \qquad \text{and} \qquad t_2 = \frac{l}{c-V} \tag{2.1}$$

where l is the distance between the transducers (0.15 m) and c is the speed of sound in air. The wind velocity and the speed of sound can be determined explicitly:

$$V = \frac{l}{2}\left(\frac{1}{t_1} - \frac{1}{t_2}\right) \tag{2.2}$$

$$c = \frac{l}{2}\left(\frac{1}{t_1} + \frac{1}{t_2}\right) \tag{2.3}$$

Once the speed of sound c is determined, the virtual temperature T_v expressed in Kelvin can be calculated by

$$T_v = \frac{c^2 + u_N{}^2}{403} \tag{2.4}$$

where both c and u_N are given in ms^{-1}, and the term

$$u_N{}^2 = v^2 + \tfrac{1}{2}(u + w)^2 \tag{2.5}$$

corrects for the curvature in the path that the sound waves travel due to air flow perpendicular to the line of the transducers (Fairall *et al.*, 1997).

2.2.3. Wave Height Measurements

The surface wave data were measured by a SeaTex Waverider buoy (Barstow *et al.*, 1991). The Waverider buoy was configured to burst sample once per hour at a 1 Hz sampling rate for a duration of approximately 17 minutes and measured motion, spectral data, and scalar wavefield parameters, including significant wave height and primary wave period T (Galbraith *et al.*, 1997). The wave dispersion equation relates the radian frequency, $\omega \equiv \frac{2\pi}{T}$, and wave number, $k \equiv \frac{2\pi}{\lambda}$, to the water depth, D:

$$\omega^2 = gk \tanh(kD) \tag{2.6}$$

where λ is the wavelength and g is the acceleration due to gravity (Earle and Bishop, 1984). Since a wave travels a distance of one wavelength in one wave period, the phase speed can be defined as

$$C_p = \frac{\lambda}{T} = \sqrt{\frac{g}{k}\tanh(kD)} \qquad (2.7)$$

Thus, with knowledge of only the water depth and the wave period, the radian frequency, wave number, and phase speed can be determined in an iterative fashion.

2.3. Marine Boundary Layer Experiment

This investigation also relies on data analyzed as part of the ONR's Marine Boundary Layers (MBL) Accelerated Research Initiative (Edson *et al.*, 1997). This program was designed to examine the 3-D structure of the marine boundary layers. The open ocean component of the MBL program was conducted off Monterey, California, in April and May of 1995 and involved the R/P FLIP, the NOAA/Oak Ridge LongEZ aircraft, and three research vessels. The emphasis of this program was on improving the understanding of flux profile relationships over the open ocean. During the field experiment, investigators deployed a 18 m mast at the end of FLIP's port booms, setting up a vertical array of 12 levels of cup/vane anemometers to provide mean profiles. Four levels of sonic anemometer/thermometers and three levels of static pressure sensors were also deployed from this mast in order to examine the flux and dissipation rate profiles and provide the necessary scaling parameters to compute the dimensionless profile functions. A single wave-wire was deployed directly beneath the mast to measure the instantaneous wave height, which was nominally 3 m beneath the lowest cup anemometer.

3. THEORY

3.1. BASIC EQUATIONS

Using the results obtained by Shaw (1990), the Navier-Stokes equations in a rotating Eulerian reference frame are

$$\frac{\partial}{\partial t}\rho u_i + \frac{\partial}{\partial x_k}\rho u_i u_k = -\frac{\partial}{\partial x_k}\left(p\delta_{ik} - \sigma'_{ik}\right) - \rho g\delta_{i3} - 2\rho\Omega\varepsilon_{ijk}\eta_j u_k \tag{3.1}$$

where

$$\sigma'_{ik} = \eta\left(\frac{\partial u_i}{\partial x_k} + \frac{\partial u_k}{\partial x_i} - \frac{2}{3}\frac{\partial u_l}{\partial x_l}\delta_{ik}\right) + \xi\frac{\partial u_l}{\partial x_l}\delta_{ik} = \sigma_{ik} + p\delta_{ik} \tag{3.2}$$

In this expression, η is the dynamic viscosity, Ω is the angular velocity of the earth, η_j is a unit vector along the axis of rotation, σ_{ik} defines the stress tensor, and ξ is a second molecular viscosity which applies to compressible flow. In general, the atmosphere boundary layer may be treated as incompressible flow and the Boussinesq approximations may be applied (Panofsky and Dutton, 1984). This reduces the continuity equation

$$\frac{\partial \rho}{\partial t} + \frac{\partial}{\partial x_i}\rho u_i = 0 \tag{3.3}$$

to

$$\frac{\partial u_i}{\partial x_i} = 0 \tag{3.4}$$

Applied to equation (3.1), these approximations yield

$$\frac{\partial u_i}{\partial t} + u_k\frac{\partial u_i}{\partial x_k} + 2\Omega\varepsilon_{ijk}\eta_j u_k = -\frac{1}{\rho}\frac{\partial p}{\partial x_i} - g\delta_{i3} + \nu\frac{\partial^2 u_i}{\partial x_k \partial x_k} \tag{3.5}$$

where $\nu \equiv \eta/\rho$ is the kinematic viscosity (Shaw, 1990).

The first law of thermodynamics applied to a fluid provides the general equation of heat transfer

$$\rho T\left(\frac{\partial s}{\partial t}+u_j\frac{\partial s}{\partial x_j}\right)=\sigma'_{ik}\frac{\partial u_i}{\partial x_k}+\frac{\partial}{\partial x_k}k_c\frac{\partial T}{\partial x_k}-\frac{\partial R_k}{\partial x_k} \tag{3.6}$$

R_k is the radiative flux; k_c is the molecular conductivity; and s is entropy, for which changes can be expressed in terms of the standard definitions of specific heat at constant pressure c_p and the equation of state

$$Tds=c_p dT-\frac{1}{\rho}dp \tag{3.7}$$

A common expression for the equation of state is

$$p=\rho R_d T_v \tag{3.8}$$

where R_d is the gas constant for dry air and T_v is virtual temperature, a function of specific humidity q.

Substituting from the equation of state, defining the potential temperature θ as $\theta\equiv T(1000/p)^{R/c_p}$ where T is in Kelvin and the pressure is given in millibars, integrating equation (3.7), and neglecting the term representing mechanical-to-thermal energy conversion transforms equation (3.6) to

$$\frac{d\theta}{dt}=\frac{\partial\theta}{\partial t}+u_k\frac{\partial\theta}{\partial x_k}=\frac{\theta}{T}\frac{k_c}{\rho c_p}\frac{\partial^2 T}{\partial x_k\partial x_k}-\frac{1}{\rho c_p}\frac{\theta}{T}\frac{\partial R_k}{\partial x_k} \tag{3.9}$$

The equation for the conservation of specific humidity q may be similarly written as

$$\frac{dq}{dt}=\frac{\partial q}{\partial t}+u_j\frac{\partial q}{\partial x_j}=D_q\frac{\partial x^2 q}{\partial x_j\partial x_j} \tag{3.10}$$

where D_q is the molecular diffusivity of water vapor.

3.2. EQUATIONS FOR TURBULENT MEAN FLOW

Equations (3.3), (3.5), (3.8), (3.9), and (3.10) form a closed set of seven equations governing seven variables. However, the equations contain nonlinear terms which render them impractical to describe turbulent flow. Instead, realizing turbulent flow as a stochastic process and applying Reynolds decomposition, which expresses the variables as a sum of a mean and fluctuating part [*i.e.*, $\phi(x,y,z,t) = \overline{\phi}(x,y,z,t) + \phi'(x,y,z,t)$], transforms equation (3.5) to

$$\begin{aligned}\frac{\partial \overline{u_i}}{\partial t} + \frac{\partial u_i'}{\partial t} + \overline{u}_j \frac{\partial \overline{u_i}}{\partial x_j} + u_j' \frac{\partial \overline{u_i'}}{\partial x_j} + \overline{u}_j \frac{\partial u_i'}{\partial x_j} + u_j' \frac{\partial u_i'}{\partial x_j} = -\frac{1}{\overline{\rho}} \frac{\partial \overline{p}}{\partial x_i} - \frac{1}{\overline{\rho}} \frac{\partial p'}{\partial x_i} \\ + \frac{\rho'}{\overline{\rho}} \frac{1}{\overline{\rho}} \frac{\partial \overline{p}}{\partial x_i} - g\delta_{i3} + \nu \frac{\partial (\overline{u}_i + u_i')}{\partial x_j \partial x_j} - 2\Omega \varepsilon_{ijk} \eta_j \overline{u_k} - 2\Omega \varepsilon_{ijk} \eta_j u_k'\end{aligned} \tag{3.11}$$

Ensemble averaging (3.11) yields the balance for mean momentum in a turbulent atmosphere:

$$\frac{\partial \overline{u_i}}{\partial t} + \overline{u}_j \frac{\partial \overline{u_i}}{\partial x_j} + 2\Omega \varepsilon_{ijk} \eta_j \overline{u_k} = -\frac{1}{\overline{\rho}} \frac{\partial \overline{p}}{\partial x_i} + \nu \frac{\partial}{\partial x_j} \frac{\partial \overline{u_i}}{\partial x_j} - \frac{\partial \overline{u_i' u_j'}}{\partial x_j} \tag{3.12}$$

The last term on the left-hand side of (3.12) represents acceleration and the Coriolis effect. The first term on the right-hand side is the pressure gradient force, and the second term is the frictional force due to molecular viscosity. The last term represents the drag resulting from momentum transfer by turbulence and is the kinematic form of the divergence of the Reynolds stress tensor,

$$\tau_{ij} = -\overline{\rho} \overline{u_i' u_j'} \tag{3.13}$$

For boundary layer studies the most important terms of the Reynolds stress tensor represent the vertical transport of horizontal momentum, defined as

$$\tau = -\overline{\rho}\left[\hat{i}\overline{u'w'} + \hat{j}\overline{v'w'}\right] \tag{3.14}$$

Determining the means to best parameterize this flux is the main focus of this thesis and will be discussed in detail in the following Chapter.

The same Reynolds decomposition and ensemble averaging procedure that were applied to equation (3.5) can be applied to the potential temperature and water vapor balances to yield

$$\frac{\partial\overline{\theta}}{\partial t} + \overline{u}_j\frac{\partial\overline{\theta}}{\partial x_j} = -\frac{\partial\overline{u_j'\theta'}}{\partial x_j} - \frac{1}{\overline{\rho}c_p}\frac{\overline{\theta}}{\overline{T}}\frac{\partial R_k}{\partial x_k} \tag{3.15}$$

and

$$\frac{\partial\overline{q}}{\partial t} + \overline{u}_j\frac{\partial\overline{q}}{\partial x_j} = -\frac{\partial\overline{u_j'q'}}{\partial x_j} \tag{3.16}$$

3.3. Equations for Turbulent Kinetic Energy

An expression for the time rate of change of the Reynolds stress tensor may be formed by subtracting (3.12) from (3.11) and applying the hydrostatic and Boussinesq approximations:

$$\frac{\partial u_i'}{\partial t} + \overline{u}_j\frac{\partial u_i'}{\partial x_j} + u_j'\frac{\partial\overline{u_i}}{\partial x_j} + u_j'\frac{\partial u_i'}{\partial x_j} = -\frac{1}{\overline{\rho}}\frac{\partial p'}{\partial x_i} + \frac{T_v'}{\overline{T}_v}g\delta_{i3} + \nu\frac{\partial^2 u_i'}{\partial x_j\partial x_j} + \frac{\partial\overline{u_i'u_j'}}{\partial x_j} \tag{3.17}$$

The relation for u_p' can be written

$$\frac{\partial u_p'}{\partial t} + \overline{u}_q\frac{\partial u_p'}{\partial x_q} + u_q'\frac{\partial\overline{u_p}}{\partial x_q} + u_q'\frac{\partial u_p'}{\partial x_q} = -\frac{1}{\overline{\rho}}\frac{\partial p'}{\partial x_p} + \frac{T_v'}{\overline{T}_v}g\delta_{p3} + \nu\frac{\partial^2 u_p'}{\partial x_q\partial x_q} + \frac{\partial\overline{u_p'u_q'}}{\partial x_q} \tag{3.18}$$

Note that the Coriolis term is not included because scale analysis shows that turbulent velocity fluctuations occur at time scales too short to be influenced by the Coriolis force (Shaw, 1990). Multiplying (3.17) by u_p' and (3.18) by u_i', averaging both equations and

adding them yields the equation for the time rate of change of the Reynolds stress tensor

$$\frac{\partial}{\partial t}\overline{u_i'u_p'} = -\overline{u_j}\frac{\partial \overline{u_i'u_p'}}{\partial x_j} - \overline{u_j'u_p'}\frac{\partial \overline{u_i}}{\partial x_j} - \overline{u_j'u_i'}\frac{\partial \overline{u_p}}{\partial x_j} - \frac{\partial}{\partial x_j}\overline{u_i'u_j'u_p'} - \frac{1}{\overline{\rho}}\left(\overline{u_p'\frac{\partial p'}{\partial x_i}} + \overline{u_i'\frac{\partial x_p'}{\partial x_j}}\right)$$
$$+ \frac{g}{\overline{T_v}}\left(\overline{u_i'T_v'}\delta_{3i} + \overline{u_p'T_v'}\delta_{3p}\right) + \nu\left(\frac{\partial^2 \overline{u_i'u_p'}}{\partial x_j \partial x_j} - 2\overline{\frac{\partial u_i'}{\partial x_j}\frac{\partial u_p'}{\partial x_j}}\right) \tag{3.19}$$

Using the notation in Shaw (1990), the mean kinetic energy of turbulence (TKE) per unit volume is defined as

$$E = \frac{1}{2}\overline{\rho}\,\overline{u_i'u_i'} \tag{3.20}$$

Alternately, meteorologists generally use the kinematic form to define the TKE

$$\overline{e} \equiv \frac{E}{\overline{\rho}} = \frac{1}{2}\overline{u_i'u_i'} \tag{3.21}$$

and the instantaneous net contribution to the TKE

$$e' \equiv \frac{1}{2}u_i'u_i' \tag{3.22}$$

The equation for rate of change of the turbulence kinetic energy follows directly from (3.19) by setting $p=i$ and making use of the continuity equation:

$$\frac{\partial \overline{e}}{\partial t} = -\overline{u_j}\frac{\partial \overline{e}}{\partial x_j} - \overline{u_i'u_j'}\frac{\partial \overline{u_i}}{\partial x_j} + \frac{g}{\overline{T_v}}\overline{u_i'T_v'}\delta_{3i} - \frac{\partial \overline{u_j'e'}}{\partial x_j} - \frac{1}{\overline{\rho}}\frac{\partial \overline{u_i'p'}}{\partial x_i} - \nu\overline{\frac{\partial u_i'}{\partial x_j}\frac{\partial u_i'}{\partial x_j}} \tag{3.23}$$

The first term of the right hand side of the equation represents the rate of change of TKE due to advection. The second term represents the generation of mechanical turbulence through shear, while the third term represents buoyancy production. The fourth and fifth terms are transport terms which neither produce nor consume energy, but act to redistribute TKE within the boundary layer; the first transport term represents the divergence of turbulent kinetic energy flux, and the second is due to the divergence of

pressure-velocity covariance. The last term is always negative and represents the dissipation ε of turbulent kinetic energy at the smallest scales due to viscous forces.

The energy budget simplifies greatly under horizontally homogeneous conditions for which mean quantities depend only on the vertical coordinate. Furthermore, since we expect the smallest scales of motion to have an isotropic structure, the expression for dissipation can also be simplified. Replacing u_i and x_i by (u,v,w) and (x,y,z), respectively, in equation (3.23), the TKE budget equation for stationary, horizontally homogeneous conditions with zero subduction $(\overline{w} = 0)$ becomes

$$-\overline{u'w'}\frac{\partial \overline{u}}{\partial z} - \overline{v'w'}\frac{\partial \overline{v}}{\partial z} + \frac{g}{\overline{T}_v}\overline{w'T_v'} - \frac{1}{\overline{\rho}}\frac{\partial \overline{w'p'}}{\partial z} - \frac{\partial \overline{w'e'}}{\partial z} - \varepsilon = 0 \qquad (3.24)$$

This is the form of the TKE budget that will be used in the following discussions.

4. METHODOLOGY

There are four standard methods for determining the momentum flux from atmospheric information:

(i) direct covariance (eddy correlation);

(ii) mean profiles;

(iii) bulk aerodynamic; and,

(iv) direct / inertial dissipation.

4.1. DIRECT TECHNIQUES TO DETERMINE THE MOMENTUM FLUX

4.1.1. DIRECT COVARIANCE (EDDY CORRELATION) METHOD

The direct covariance method is the standard upon which all other methods of estimating the momentum flux are based. Whereas the other three methods rely on similarity theory, the covariance method is a direct computation of the Reynolds stress and yields an unbiased estimate of the flux (Fairall *et al.*, 1990). Revisiting equation (3.14), the wind stress can be determined directly by measuring the turbulent components of the streamwise and vertical wind velocity:

$$\tau = -\overline{\rho}\left[\hat{i}\overline{u'w'} + \hat{j}\overline{v'w'}\right] \tag{4.1}$$

In practice, the ensemble average is approximated by averaging simultaneous measurements of the turbulent components of wind velocity and cross correlating them over a finite time interval (Frederickson *et al.*, 1997). The assumption that allows us to relate time averaged fluxes to ensemble averaged fluxes is referred to as ergodicity (Panofsky and Dutton, 1984). For stationary conditions, as the length of the averaging

interval increases, the accuracy of this approximation generally increases, although there is a tradeoff between the choice of averaging period and nonstationarity of the data (Mahrt *et al.*, 1996).

The primary disadvantage of the direct covariance method is that comparative studies (*e.g.*, Fairall *et al.*, 1990; Edson *et al.*, 1991; Edson and Fairall, 1998) indicate that the direct covariance method is highly susceptible to flow distortion. Additionally, unless the measurements are made from a stable platform, such as a fixed mast or tower, the data must be corrected for platform motion contamination. Clearly, this limits the applicability of this method from ships and buoys.

4.1.2. Motion-Corrected Covariance Method

However, a great deal of effort has been made in recent years to compute direct covariance fluxes from moving platforms to improve flux parameterizations over the open ocean (*e.g.*, Fujitani, 1981, 1985; Tsukamoto, 1990; Dugan *et al.*, 1991; Anctil *et al.*, 1994; Fairall *et al.*, 1997; Edson *et al.*, 1998). If one wishes to apply the direct covariance method on a moving platform, then the orientation and motion of the platform must be accounted for before computing the correlations (Fairall *et al.*, 1990). Surface-following buoys experience a variety of motions including instantaneous tilt of the sensors due to platform movement, angular velocities about the platform's local coordinate system, and translational velocities with respect to a fixed frame of reference (Fujitani, 1981; Hare *et al.*, 1992). In vector notation, the motion corrected wind speed $\vec{V}_{true}$ can be written as

$$\vec{V}_{true} = \mathbf{T}\left(\vec{V}_{obs} + \vec{\Omega}_b \times \vec{R}\right) + \vec{V}_{mot} \tag{4.2}$$

where **T** is the rotation matrix which transforms measurements taken in the buoy reference frame to earth coordinates; $\vec{V}_{obs}$ and Ω_b are the measured wind speeds and angular rates in the buoy frame of reference, respectively; $\vec{R}$ is the position vector of the wind sensor with respect to the motion package; and, $\vec{V}_{mot}$ represents the translational velocities in the fixed frame (Anctil *et al.*, 1994; Edson *et al.*, 1998). The product $\vec{\Omega}_b \times \mathbf{T}\vec{R}$ represents the angular velocity in the fixed frame.

Removal of this motion from our wind sensors requires us to measure the three dimensional translational motion of a reference point on the buoy, the three angular rotations about that point, and the Euler angles required for the transformation matrix. During the CMO experiment, three Systron Donner quartz sensors recorded the pitch, roll, and yaw rates ($\dot{\Phi}$, $\dot{\Theta}$, and $\dot{\Psi}$, respectively), and a three-axis Columbia linear servo accelerometer provided the linear accelerations of the buoy ($\ddot{x}$, $\ddot{y}$, and $\ddot{z}$, respectively). All of the sensors were strapped down in the hull of the discus buoy. One of the main advantages of a strap-down system is that it readily computes the angular rates in the buoy frame of reference:

$$\vec{\Omega}_b = \left[\dot{\Phi}\hat{\mathrm{i}} + \dot{\Theta}\hat{\mathrm{j}} + \dot{\Psi}\hat{\mathrm{k}}\right] \tag{4.3}$$

where $\hat{i}$, $\hat{j}$, and $\hat{k}$ represent the unit vectors in a right-hand coordinate system pointing from the buoy fin to front, starboard to port, and vertically up, respectively.

The three Euler angles which specify the rotation of the buoy are the pitch Φ, roll Θ, and yaw Ψ. Using the approach described by Edson *et al.* (1998), the Euler angles are approximated using complimentary filtering, which combines the high-passed filtered integrated angular rates with the low-passed linear accelerations as

$$\Phi \approx \frac{1}{\tau+1}\frac{\ddot{y}}{g}+\frac{\tau s}{\tau s+1}\Phi \tag{4.4}$$

$$\Theta \approx \frac{1}{\tau+1}\frac{\ddot{x}}{g}+\frac{\tau s}{\tau s+1}\Theta \tag{4.5}$$

and

$$\Psi \approx \frac{1}{\tau+1}\Psi_{slow}+\frac{\tau s}{\tau s+1}\Psi \tag{4.6}$$

where s represents the differentiation operator such that $\dot{\Phi} = s\Phi$, τ is a time constant, Ψ_{slow} represents the compass output, and a small angle approximation is made in (4.4) and (4.5).

Given the Eulerian angles, the rotation matrix $\mathbf{T}$ which transforms measurements taken in the buoy reference frame to earth coordinates can be expressed:

$$\mathbf{T} = \begin{bmatrix} \cos\Psi\cos\Theta & -\sin\Psi\cos\Phi+\cos\Psi\sin\Theta\sin\Phi & \sin\Psi\sin\Phi+\cos\Psi\sin\Theta\cos\Phi \\ \sin\Psi\cos\Theta & \cos\Psi\cos\Phi+\sin\Psi\sin\Theta\sin\Phi & \sin\Theta\cos\Phi\sin\Psi-\sin\Phi\cos\Psi \\ -\sin\Theta & \cos\Theta\sin\Phi & \cos\Theta\cos\Phi \end{bmatrix} \tag{4.7}$$

Again, the sign convention corresponds to a right-handed coordinate system with Ψ positive for the ship's bow yawed counter-clockwise from north, Φ positive for the port side rolled up, and Θ positive for the bow pitched down (Edson *et al.*, 1998).

The accelerations are then rotated into the vertical using the rotation matrix $\mathbf{T}$ before adding the gravity vector, $\vec{g} = (0,0,-g)$, to the rotated accelerations. The resulting accelerations are then high-pass filtered to remove any drift before integrating. This process can be expressed as:

$$\vec{V}(t)_{mot} = \int\left[Hp\left(T\vec{\ddot{x}}(t)+\vec{g}\right)\right]dt \tag{4.8}$$

where *Hp* represents a high-pass filter operator. The strapped-down system thereby provides all the terms required by (4.2) to compute the true wind velocity. These corrected velocities are then used to compute the wind stress.

4.2. Indirect Techniques to Determine the Momentum Flux

Monin and Obukhov (1954) postulated that the turbulent fluxes of atmospheric momentum and heat energy in a stationary, horizontally homogeneous surface layer is determined by the height above the surface *z*, the buoyancy parameter $g/\overline{\theta_V}$, the friction velocity u_*, and the surface buoyancy flux $\overline{w'\theta'_{V0}}$ where $\overline{\theta_V}$ is the virtual potential temperature and accounts for density changes due to humidity fluctuations and *g* is the acceleration of gravity (Lumley and Panofsky, 1963; Wyngaard, 1973). The friction velocity u_* is defined in the manner of equation (4.1) from the surface stress:

$$u_* = \left[\frac{|\tau_0|}{\rho}\right]^{\frac{1}{2}} = \left[\left(-\overline{u'w'}\right)^2 + \left(-\overline{v'w'}\right)^2\right]^{\frac{1}{4}} \tag{4.9}$$

Largely on the basis of dimensional arguments, Monin-Obukhov (MO) similarity theory predicts that the various terms in the TKE budget [equation (3.24)] are universal functions of the MO stability parameter ζ after normalization by the appropriate scaling parameter, $\frac{\kappa z}{u_*^3}$:

$$\frac{\varepsilon \kappa z}{u_*^3} = \phi_\varepsilon(\zeta) = \phi_M(\zeta) - \zeta - \phi_{tp}(\zeta) - \phi_{te}(\zeta) \tag{4.10}$$

where κ is the dimensionless von Kármán constant, generally assumed to be 0.4 (Högström, 1987; Edson *et al.*, 1991; Fairall *et al.*, 1996a); ϕ_ε is the dimensionless

dissipation function; ϕ_{tp} and ϕ_{te} are the dimensionless transport terms; and, ϕ_M is the dimensionless shear defined as

$$\phi_M(\zeta) = \frac{\kappa z}{u_*}\left[\left(\frac{\partial \overline{u}}{\partial z}\right)^2 + \left(\frac{\partial \overline{v}}{\partial z}\right)^2\right]^{1/4} \tag{4.11}$$

The stability parameter ζ represents the ratio of the height above the surface z to the Monin-Obukhov length L defined as $L \equiv -\frac{\overline{\theta_V}}{g\kappa}\frac{u_*^3}{\overline{w\theta_V}_0}$, such that $\zeta \equiv \frac{z}{L}$. In unstable conditions the Monin-Obukhov length represents the height where mechanical and buoyant production of turbulence are approximately equal, *i.e.*, at this height, $\zeta = -1$. At heights below this level, shear production dominates; while above this level, buoyancy dominates. In stable conditions the stratification consumes some of the kinetic energy such that ζ represents the ratio of buoyant consumption to shear production.

4.2.1. MEAN PROFILE METHOD

Generally, the wind direction is assumed to be constant in the surface layer such that the coordinate system is rotated so that $\overline{v} = 0$. In this coordinate system the wind shear becomes

$$\frac{\partial \overline{u}}{\partial z} = \frac{u_*}{\kappa z}\phi_M(\zeta) \tag{4.12}$$

Upon integrating the above equation, one obtains the logarithmic wind profile for neutral conditions upon which the profile method is based:

$$\overline{u}(z) = \overline{u}(z_0) + \frac{u_*}{\kappa}\left[\ln\left(\frac{z}{z_0}\right) - \psi_M\left(\frac{z}{L}\right)\right] \tag{4.13}$$

where z_0 is the aerodynamic roughness length and reflects the roughness of the surface, and ψ_M is the integrated form of ϕ_M. Using equation (4.13), it is relatively easy to obtain u_* and z_0 from a given wind profile: plotting u as a function of $\ln(z) - \psi_M(\zeta)$ results in a straight line with $\frac{u_*}{\kappa}$ as the slope and $\frac{u_*}{\kappa}\ln(z_0)$ as the intercept.

Therefore, the implementation of the profile method requires the deployment of multiple sensors at varying heights. This type of deployment in the marine surface layer creates a number of problems. In addition to the cost associated with employing an array of sensors, excellent relative calibration among sensors is required due to the small shear found over the ocean. Additionally, calibration drift between the individual sensors due to mechanical degradation may result in large uncertainties among measurements. Another physical limitation of the profile method is the requirement for the lowest sensor to be at least two or three wave heights above the interface since the presence of undulating long waves causes deviations to the logarithmic profile (Geernaert, 1990). This requirement further limits the placement of the sensors since they upper height is already bounded by the height of the surface layer, the region within which the fluxes vary by no more than 10% of their surface values, a requirement of MO similarity theory. Finally, and probably most importantly, the physical set-up of the array renders the sensors extremely sensitive to flow distortion and motion contamination. Therefore, this method has rarely been implemented over the ocean.

4.2.2. BULK AERODYNAMIC METHOD

The bulk method is the simplest and most widely used of the four techniques. The bulk method is an application of the profile method for which the structure of the atmospheric boundary layer is estimated by using measurements at one level and assuming a logarithmic wind profile. The standard bulk expression for the stress components is

$$\tau_{0i} = \rho u_*^2 = \rho_a C_D \left(\overline{u_i}(z) - \overline{u_i}(z_0)\right)\left|\overline{u_i}(z) - \overline{u_i}(z_0)\right| \tag{4.14}$$

where C_D is the bulk transfer coefficient for stress; $\overline{u_i}(z)$ is the average of one of the horizontal wind components relative to the fixed Earth measured at some reference height z; and $u_i(z_0)$ is the surface current (Fairall *et al.*, 1996a). The velocity difference is, therefore, the velocity relative to the ocean surface.

Equation (4.14) can then be used to define the drag coefficient as

$$C_D(z) = \left[\frac{\kappa}{\log(z/z_0) - \psi_M(\zeta)}\right]^2 \tag{4.15}$$

The neutral drag coefficient is related to the roughness length by

$$C_{DN}(z) = \left[\frac{\kappa}{\log(z/z_0)}\right]^2 \tag{4.16}$$

such that

$$(C_{DN})^{1/2} = \frac{C_D^{1/2}}{1 + \frac{\psi_M(\zeta)}{\kappa}(C_D)^{1/2}} \tag{4.17}$$

where the subscript N denotes the value in neutral conditions; and, $\psi_M(\zeta)$ is the MO similarity profile function. The following expressions of Businger *et al.* (1971) and Dyer

(1974) are the most commonly used:

$$\psi_M(\zeta) = (1-16\zeta)^{-1/4} \qquad \zeta < 0 \tag{4.18a}$$

$$\psi_M(\zeta) = (1+5\zeta) \qquad \zeta \geq 0 \tag{4.18b}$$

Using the approach described by Smith (1988), the velocity aerodynamic roughness length z_0 can be expressed as

$$z_0 = z_s + z_r \tag{4.19}$$

where z_s and z_r represent the aerodynamic roughness of smooth and rough flows, respectively. The roughness length for a smooth surface depends on the viscosity of air ν and the friction velocity (Businger, 1973):

$$z_s = \frac{\nu}{9u_*} \tag{4.20}$$

The determination of z_r is based on the relationship proposed by Charnock (1955). Using dimensional analysis, Charnock assumed that the aerodynamic roughness length of the surface for well-developed seas is proportional to the wind stress which generates and supports the surface waves and gravity which acts as the restoring force:

$$z_r = \frac{\alpha_c u_*^{\,2}}{g} \tag{4.21}$$

where α_c is the Charnock "constant" for which values between 0.010 and 0.035 can be found in the literature (Garratt, 1992). Representing the ratio of inertial force to gravitational force, the Charnock constant is analogous to a Froude number.

The method and algorithm for computing the bulk estimates are described in detail in Fairall *et al.* (1996a). In summary, the bulk estimates are calculated by using the

roughness length described above with a Charnock constant of 0.011 and with the following corrections:

(i) In highly unstable conditions, $\zeta \equiv \frac{z}{L} << -1$, the profiles of temperature, moisture,

and momentum are altered so that they obey the $\zeta^{-1/3}$ asymptotic convective limit dependence on stability (Wyngaard, 1973).

(ii) A gustiness velocity $w_g \equiv \beta W_*$ is used in the computation of the mean wind speed. β is an empirical constant of the order of 1.0, and the convective velocity W_* is computed as follows:

$$W_*^3 = \frac{g}{T}\left[\frac{Q_H}{\rho_a c_{pa}} + 0.61T\frac{Q_E}{\rho_a L_e}\right] z_i \tag{4.22}$$

where Q_H and Q_E are the sensible and latent heat fluxes, respectively; ρ_a and c_{pa} are the density and isobaric specific heat of air; L_e is the latent heat of vaporization; T is the potential temperature at the surface; and z_i is the depth of the convective boundary layer (approximately 600 m). This factor accounts for the appreciable momentum flux observed in highly convective conditions where the mean wind shear goes to zero but its variance (*i.e.*, gustiness) does not.

(iii) The "Webb" correction (Webb *et al.*, 1980), which accounts for variations in air density due to the presence of a heat flux, is applied.

(iv) Cool-skin correction as described by Fairall *et al.* (1996b) for nonradiative sea surface temperature measurements is incorporated. Note that since the temperature sensor was at 1.5 m, no warm layer correction was applied due to the shallow depth.

One potential source of error in the bulk aerodynamic method is in the characterization of the roughness length by equations (4.19) through (4.21). Charnock's expression for the roughness of the sea surface has been shown to be generally valid for moderate to high wind speeds at unlimited fetch and duration (Geernaert *et al.*, 1986). However, upon examining equation (4.21), one sees that no characteristics of the wave field are truly present. This implicitly assumes that the wind and wave fields are in local equilibrium; consequently, Charnock's relation will only give consistent results for a fully-developed sea (Donelan, 1990; Maat *et al.*, 1991; Dobson *et al.*, 1994). Sudden changes in the wind, such as that due to frontal passages, result in the wind field being temporarily out of equilibrium with the existing wave field (Smith, 1988). The momentum transfer between the wind and wave fields as the waves grow or decay in response to the forcing is not considered in Charnock's expression. Additionally, the influence of varying fetch and possible interactions with the bottom in shallow water are not included. The neglect of these processes probably explains the wide range of values for the Charnock's "constant" found from different experiments. Finally, implementation of the bulk aerodynamic method using buoy data often places the measurements where the waves cause changes to the log profile. All of these effects result in changes to the drag coefficient which are sea-state dependent.

4.2.3. Direct and Inertial Dissipation Methods

The direct dissipation and the inertial dissipation methods differ only in the manner in which the dissipation rate for turbulent kinetic energy is computed. Direct measurements of dissipation rates are determined by integrating over the spectrum of the velocity derivatives (Fairall and Larsen, 1986):

$$\varepsilon = 15\nu\left(\overline{\frac{\partial u'}{\partial x}}\right)^2 \approx \frac{15\nu}{\overline{u}^2}\left(\overline{\frac{\partial u'}{\partial t}}\right)^2 \tag{4.23}$$

Since the fluctuations have a spatial resolution that approaches the Kolmogorov microscale (typically 1 mm in atmospheric flows), hot-wire anemometers must be used to obtain direct measurements (Edson and Fairall, 1998). While this method has been used overland, its applicability over the ocean is limited due to contamination and even destruction of the wires by sea spray (Edson and Fairall, 1998). Therefore, the direct dissipation method is rarely employed over the ocean.

Instead, the inertial subrange method, which requires frequency responses only up to the order of 10-100 Hz, is more commonly employed (Smith *et al.*, 1996; Fairall *et al.*, 1997). In the inertial subrange of local isotropic turbulence, the one-dimensional velocity variance spectrum Φ_u can be expressed as a function of wavenumber magnitude as

$$\Phi_u(k) = \alpha_u \varepsilon^{2/3} k^{-5/3} \tag{4.24}$$

where α_u is the one-dimensional Kolmogorov constant, taken to be 0.52 (Högström, 1996), and k is the wavenumber.

Invoking Taylor's frozen turbulence hypothesis, $k \equiv \frac{2\pi f}{\overline{U_s}} \equiv \frac{\omega}{\overline{U_s}}$, the velocity variance spectra can be related to the frequency spectra S_u as

$$k\Phi_u(k) = \frac{fS_u(f)}{(T_{uu})(Q_{uu})(att_1 + att_2)} = \alpha_u \varepsilon^{2/3}\left(\frac{2\pi f}{\overline{U_s}}\right)^{-2/3} \tag{4.25}$$

where f is frequency, S_u is the spectrum of the streamwise velocity $\overline{U_s}$ as a function of the angular frequency ω, and T_{uu} and $(att_1 + att_2)$ are correction factors:

(i) T_{uu} is a correction for inaccuracies in using Taylor's hypothesis to estimate the magnitude of wavenumber spectra in the inertial subrange and has the form given by Wyngaard and Clifford (1977):

$$T_{uu} = 1 - \frac{1}{9}\frac{(\sigma_u)^2}{\overline{U}_s^2} + \frac{2}{3}\frac{\left(\sigma_v^2 + \sigma_w^2\right)}{\overline{U}_s^2} \tag{4.26}$$

where σ_u^2, σ_v^2, σ_w^2 are variances (uu, vv and ww) computed from the same time series that produced the spectral estimate (Hill, 1996).

(ii) The terms att_1 and att_2 correct for excess damping of higher frequencies caused by the eight-fold pulse-averaging of the sonic anemometer (Henjes *et al.*, 1998) and has the forms

$$att_1 = \frac{\sin^2\left(\frac{\pi f}{f_0}\right)}{\left(\frac{\pi f}{f_0}\right)^2} \tag{4.27a}$$

$$att_2 = \left(\frac{f}{f_0 - f}\right)^{5/3}\left(\frac{\sin^2\left[\frac{\pi(f_0 - f)}{f_0}\right]}{\left[\frac{\pi(f_0 - f)}{f_0}\right]^2}\right)\left(\frac{\sin^2\left[\frac{\pi l(f_0 - f)}{\overline{U}_s}\right]}{\left[\frac{\pi l(f_0 - f)}{\overline{U}_s}\right]^2}\right) \tag{4.27b}$$

where f_0 is the Nyquist frequency, 20.833 Hz.

Note that spatial averaging also reduces the spectral estimates at high frequencies, in the manner described by Kaimal *et al.* (1968):

$$Q_{uu} = \frac{\sin^2\left(\frac{kl}{2}\right)}{\left(\frac{kl}{2}\right)^2} \tag{4.28}$$

where l is the separation distance between the sonic heads. However, the effect of line-averaging is negligible for $kl < 1$. Since we have limited the frequency range such that $f < \frac{\overline{U_s}}{2\pi l}$, this correction is not needed.

When using the inertial dissipation method, it is generally assumed that the transport terms cancel (Hicks and Dyer, 1972; Large and Pond, 1981; Dyer and Hicks, 1982; Large and Businger, 1988) so that a balance exists between the viscous dissipation and production (buoyant and shear) of TKE. Under this assumption, equation (4.10) reduces to

$$\frac{\varepsilon \kappa z}{u_*^3} = \phi_\varepsilon(\zeta) \approx \phi_M(\zeta) - \zeta \tag{4.29}$$

A potential source of error in using the inertial dissipation technique arises from the assumption that there is a balance between TKE production and dissipation. Recent investigations (Vogel and Frenzen, 1992; Frenzen and Vogel, 1992; Thiermann and Grassl, 1992; Yelland and Taylor, 1996; Edson *et al.*, 1997; Edson and Fairall, 1998) suggest that there is a local imbalance between the pressure and energy transport terms such that the magnitude of the energy transport term $\phi_{te}(\zeta)$ is greater than the magnitude of the pressure transport term $\phi_{tp}(\zeta)$, and TKE production exceeds dissipation by 15-20%. Over the ocean, it has been hypothesized by Edson *et al.* (1997) that this dissipation deficit is due to the flux of energy going into ocean waves.

The flux of kinetic energy, $F(z)$, into a layer of air over a horizontally homogeneous surface is given by

$$F(z) = \overline{u'w'}u(z) + \overline{v'w'}v(z) + \overline{w'e'} + \frac{1}{\rho}\overline{w'p'} \tag{4.30}$$

where the first two terms on the right-hand side of the equation represent the flux of mean flow kinetic energy and the last two terms represent the rate of diffusion of kinetic energy (Edson *et al.*, 1997). Over land, it is generally assumed that there is no energy flux through the ground so that the flux entering the layer at height h can be related to the total rate of dissipation within the layer by

$$\int_0^h \varepsilon dz = -F(h) + \frac{g}{T_v}\int_0^h \overline{w'T_v'}dz \tag{4.31}$$

where the last term represents the generation of kinetic energy due to buoyancy flux (Edson *et al.*, 1997). For neutral conditions, equation (4.31) states that the flux of kinetic energy into the layer equals the dissipation within that layer; *i.e.*, production balances dissipation. However, over the ocean, where the exchange of momentum from the atmosphere to the ocean results in wind-driven waves and currents, the surface energy flux $F(0)$ is not negligible and the additional forcing mechanism of the surface waves must be included.

The effects of surface waves are included in the KE energy budget equation (3.24) and energy flux equation (4.30) by decomposing the velocity into mean, turbulent, and wave-induced components

$$u(t) = \bar{u} + u'(t) + \tilde{u}(t) \tag{4.32}$$

where the tilde represents the wave-induced component. The wave-induced component is defined with the use of the phase-averaging operator as described by Finnegan *et al.* (1984):

$$\langle u(t)\rangle_P = \bar{u} + \tilde{u}(t) = \lim_{N_L \to 0}\left[\frac{1}{N_L}\sum_{n=1}^{N_L} u(t + n\tau_o)\right] \tag{4.33}$$

$$\tilde{u}(t) = \langle u(t)\rangle_P - \bar{u} \tag{4.34}$$

where τ_o is the period of the organized oscillation and N_L represents the number of consecutive wavelengths averaged together to get one phase-averaged wave. This type of averaging can be used to rewrite equation (3.24) to include the wave-induced contributions. An approximation of the steady state solution of the TKE energy budget is

$$\begin{aligned} &-\left[\overline{u'w'} + \overline{\tilde{u}\tilde{w}}\right]\frac{\partial \bar{u}}{\partial z} - \left[\overline{v'w'} + \overline{\tilde{v}\tilde{w}}\right]\frac{\partial \bar{v}}{\partial z} + \frac{g}{\bar{T}_v}\left[\overline{w'T_v'} + \overline{\tilde{w}\tilde{T}_v}\right] - \frac{1}{\bar{\rho}}\left[\frac{\partial \overline{w'p'}}{\partial z} + \frac{\partial \overline{\tilde{w}\tilde{p}}}{\partial z}\right] \\ &-\left[\frac{\partial \overline{w'e'}}{\partial z} + \frac{\partial \overline{\tilde{w}\tilde{e}}}{\partial z}\right] - \varepsilon - \left[\frac{\overline{\tilde{u}_j}}{2}\frac{\partial \overline{\tilde{r}_{ii}}}{\partial x_j} + \frac{\partial \overline{\tilde{u}_i \tilde{r}_{ij}}}{\partial x_j}\right] = 0 \end{aligned} \tag{4.35}$$

where $\tilde{r}_{ii}$ and $\tilde{r}_{ij}$ can be viewed as the wavelike fluctuations in the background Reynolds stress due to the presence of waves

$$\tilde{r}_{ij} = \langle u_i' u_j' \rangle_P - \overline{u_i' u_j'} \tag{4.36}$$

such that the sum of the last two terms in brackets represents the interaction between the wave field and the wavelike part of the turbulent stresses and constitutes a loss of kinetic energy (Finnigan *et al.*, 1984). In this form, the shear production P now includes terms representing the wave-induced momentum flux,

$$P = -\left[\overline{u'w'} + \overline{\tilde{u}\tilde{w}}\right]\frac{\partial \bar{u}}{\partial z} - \left[\overline{v'w'} + \overline{\tilde{v}\tilde{w}}\right]\frac{\partial \bar{v}}{\partial z} \tag{4.37}$$

The production of kinetic energy is therefore the result of a forcing mechanism that is a function of sea state.

Similarly, the transport of energy from wind to waves at the ocean surface is actually the lower boundary condition of the pressure transport term, *i.e.*,

$$F(0) = \frac{1}{\rho}\widetilde{w}\widetilde{p}\Big|_0 \approx \frac{1}{\rho}\overline{\frac{\partial \chi}{\partial t}\, p_0} \tag{4.38}$$

where χ is the surface elevation and the time rate of change is known as the piston velocity. This term must be included in equation (4.31) in over ocean studies such that

$$\int_0^h \varepsilon dz = F(0) - F(h) + \frac{g}{T_v}\int_0^h \left[\overline{w'T_v'} + \overline{\widetilde{w}\widetilde{T}_v}\right] dz \tag{4.39}$$

where the fluxes now represents both turbulent and wave-induced fluctuations. Unlike the solid boundary for which the flux through its surface is negligible, there is a transfer of energy from the atmosphere to the ocean, and the total amount of dissipation within the wave boundary layer is expected to be less than required to balance the energy flux into the layer; a phenomenon supported by recent investigations (Yelland and Taylor, 1996; Edson *et al.*, 1997; Edson and Fairall, 1998). Thus, in the wave boundary layer, the transport of energy and momentum to the ocean from the atmosphere is not adequately described using Monin-Obukhov similarity theory, and additional scaling parameters are required for similarity.

5. ANALYSIS AND RESULTS

The objective of this analysis is to improve estimates of the momentum flux using modified forms of the bulk aerodynamic and inertial dissipation methods. The modifications to the bulk aerodynamic method involve the derivation of a roughness length parameterization which is sensitive to sea state. These modifications are drawn from comparisons with direct covariance and inertial dissipation flux estimates. In the case of the inertial dissipation momentum fluxes, additional parameterizations are applied to account for the effects of surface waves and the non-zero energy flux from the atmosphere to the ocean.

5.1. DATA SELECTION

The data sets obtained from both the VAWR sensor and sonic anemometer span the entire eleven months from August 1996 to June 1997 and represent a total of 15,262 data points (2 measurements per hour for approximately 318 days). Of these measurements a total of 2,303 points, or 15%, were removed prior to processing for one or more of the following reasons:

(i) Instrument failure (VAWR and/or sonic anemometer).

(ii) The velocity spectrum for inertial dissipation calculations did not meet the $-\frac{5}{3}$ slope criteria [see equation (4.24)] and did not allow the calculation of dissipation estimates. Possible reasons include rain and spray contamination and obstructions to the path (*e.g.*, due to a seagull sitting on the sensor).

(iii) Flow distortion, which arises when the relative wind direction is greater than $\pm 60^{o}$ from head on.

The wave height data set represents 241 days of the eleven-month deployment, but only 1 measurement per hour was taken for a total of 5,778 points. In order to insure that oceanographic conditions resulted from locally-generated seas and not from swell propagating into the test site, 8% of the wave data were discarded prior to processing because two distinct peaks were present.

For motion-corrected covariance calculations, the data set was further limited by the amount of data collected by the motion-correction package. This package collected 30 minutes of 10 Hz data at noon and midnight for 317 days which produced a data set totaling 634 direct covariance flux estimates.

5.2. Traditional Approach

Using the procedures outlined in Chapter 4, the friction velocity u_*, as defined by equation (4.9), was calculated using the bulk aerodynamic, inertial dissipation, and direct covariance methods. Figures 5.1 through 5.3 are comparisons of the u_* calculations. The inertial dissipation and bulk aerodynamic methods provide remarkably similar values for $u_* < 0.6$ m/s (Figure 5.1). At higher wind speeds, the inertial dissipation method predicts progressively higher values of u_* than the bulk aerodynamic method, although the values generally exhibit less than a 12% difference. Compared to friction velocity values computed by the motion-corrected covariance method (Figures 5.2 and 5.3), both the bulk aerodynamic and inertial dissipation methods provide u_* estimates which are consistently 7-12% lower than expected for $u_* > 0.2$ m/s. This would suggest that although the two methods provide quite similar results, these values are underestimating the actual momentum flux over the ocean.

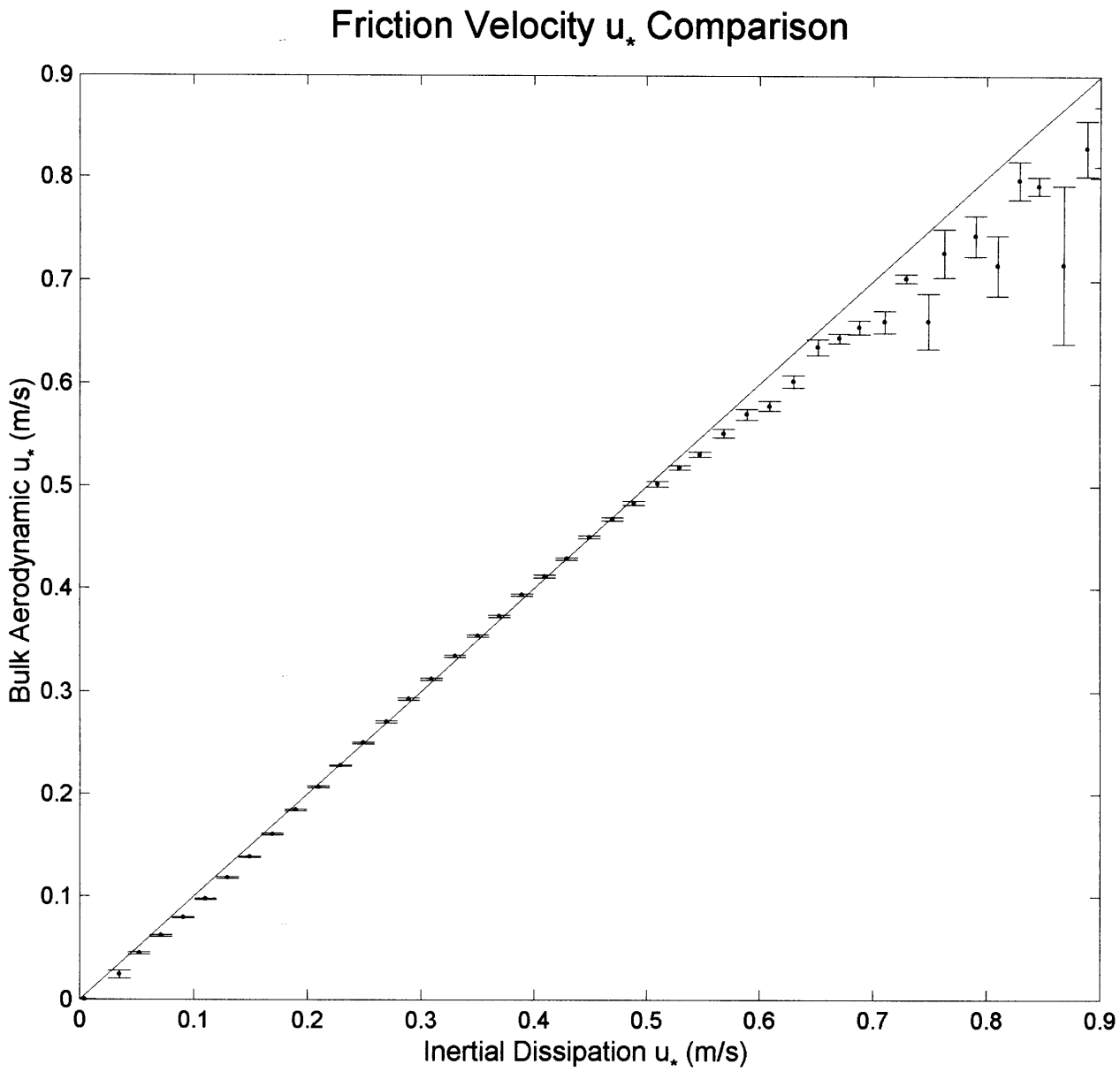

Figure 5.1 A comparison of the friction velocities, u_*, estimated using the bulk aerodynamic versus inertial dissipation methods and bin-averaged in increments of 0.02 m/s. The error bars denote the standard error (standard deviation divided by the number of points).

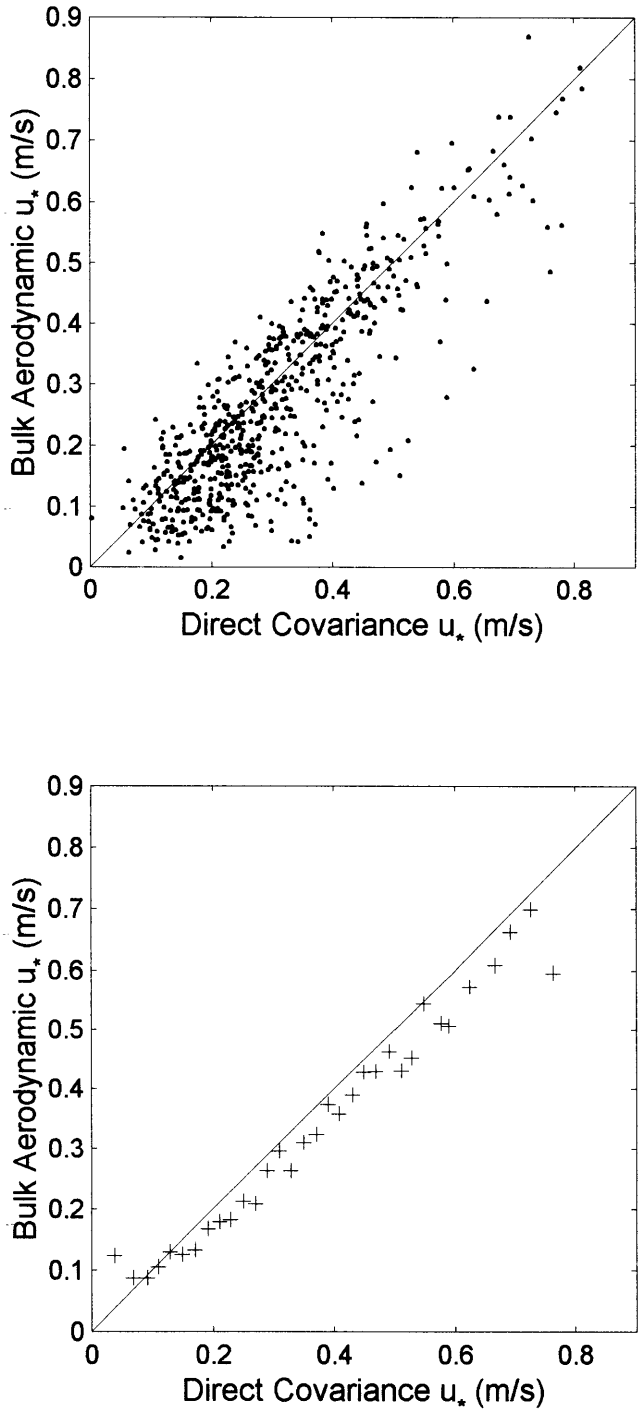

Figure 5.2 Friction velocity, u_*, comparisons of the bulk aerodynamic versus motion-corrected covariance method. Values of u_* are bin-averaged in increments of 0.02 m/s.

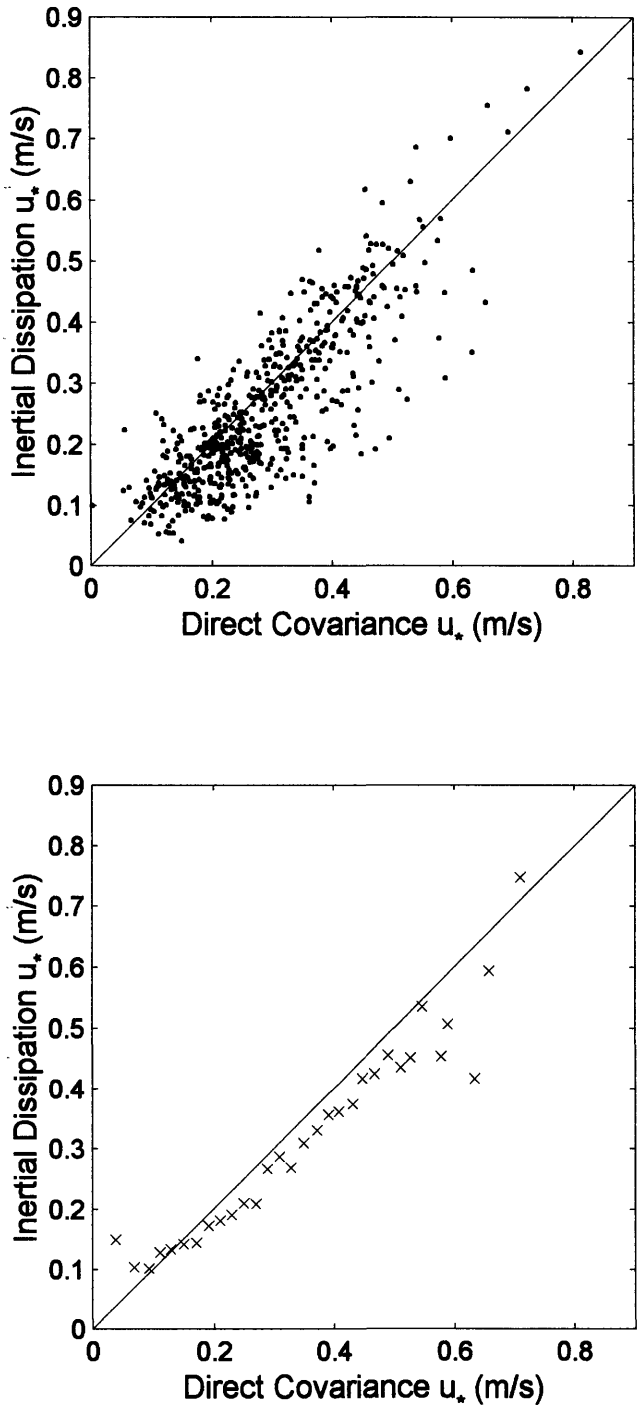

Figure 5.3 Friction velocity, u_*, comparisons of the inertial dissipation versus motion-corrected covariance method. Values of u_* are bin-averaged in increments of 0.02 m/s.

The neutral drag coefficient C_{DN} described by equation (4.17), was calculated by the bulk aerodynamic, inertial dissipation, and direct covariance methods for the following four wave-age bins:

(i) $\frac{C_p}{u_*} \leq 24$;

(ii) $24 < \frac{C_p}{u_*} \leq 28$;

(iii) $28 < \frac{C_p}{u_*} \leq 32$; and,

(iv) $32 < \frac{C_p}{u_*}$;

where C_p is the phase speed of the dominant seas, calculated using equation (2.7). The first wave-age bin corresponds to young (developing) seas, the second and third wave-age bins represent seas for which the waves receive no additional energy input from the wind and are considered fully-developed, and the last wave-age bin corresponds to waves that are decaying. [An alternate expression for the wave age is $\frac{C_p}{U_{10N}}$, where young waves correspond to $0.22 \leq \frac{C_p}{U_{10N}} \leq 0.29$ and fully-developed waves are represented by $0.5 \leq \frac{C_p}{U_{10N}} \leq 1.25$ (Donelan, 1990).] Interestingly, less than 10% of the data represent conditions in which the seas were growing. The absence of young waves from the data set most likely indicates a limit in the techniques used to detect young waves. A review

of the meteorological record reveals that the CMO test site experienced numerous frontal passages and storm systems (including two tropical storms) with wind conditions that should be associated with new wave development. One limitation is the inability of the waverider buoy to sense waves with wavelengths less than twice its diameter, about 2 m. Thus, the wind stress can only be related to the shortest-wavelength waves (4 m) sensed by the buoy. Another possibility is that new seas are masked by residual energy from large swell peaks which exist near the sea-swell transition frequency, but this hypothesis has not been explored. Dobson *et al.* (1994) reported the same lack of young seas in their data set, and both these results indicate the need for improved methods to detect and categorize seas. Nevertheless, while we are unable to distinguish the youngest waves, categorization of the seas into the four wave-age bins defined above was possible and provided invaluable insight into the relationship between the sea surface wind stress and wave state.

The bulk aerodynamic neutral drag coefficients, C_{DN}, are approximately 5-15% lower than the values measured using the direct covariance method for young seas (Figure 5.4). For decaying seas, however, the bulk estimates tend to over predict the drag coefficient by approximately the same error. As Figure 5.5 depicts, the required Charnock's "constant" to provide the best agreement for the young seas is $\alpha_c = 0.0150$; a value of $\alpha_c = 0.0126$ gives the best agreement for fully-developed seas; while a value of $\alpha_c = 0.0059$ provides the best agreement for decaying seas. The Charnock's constant which gives the best agreement when all wave-ages are considered is $\alpha_c = 0.0116$, which is in good agreement with the value obtained by Fairall *et al.* (1996a) and used in the

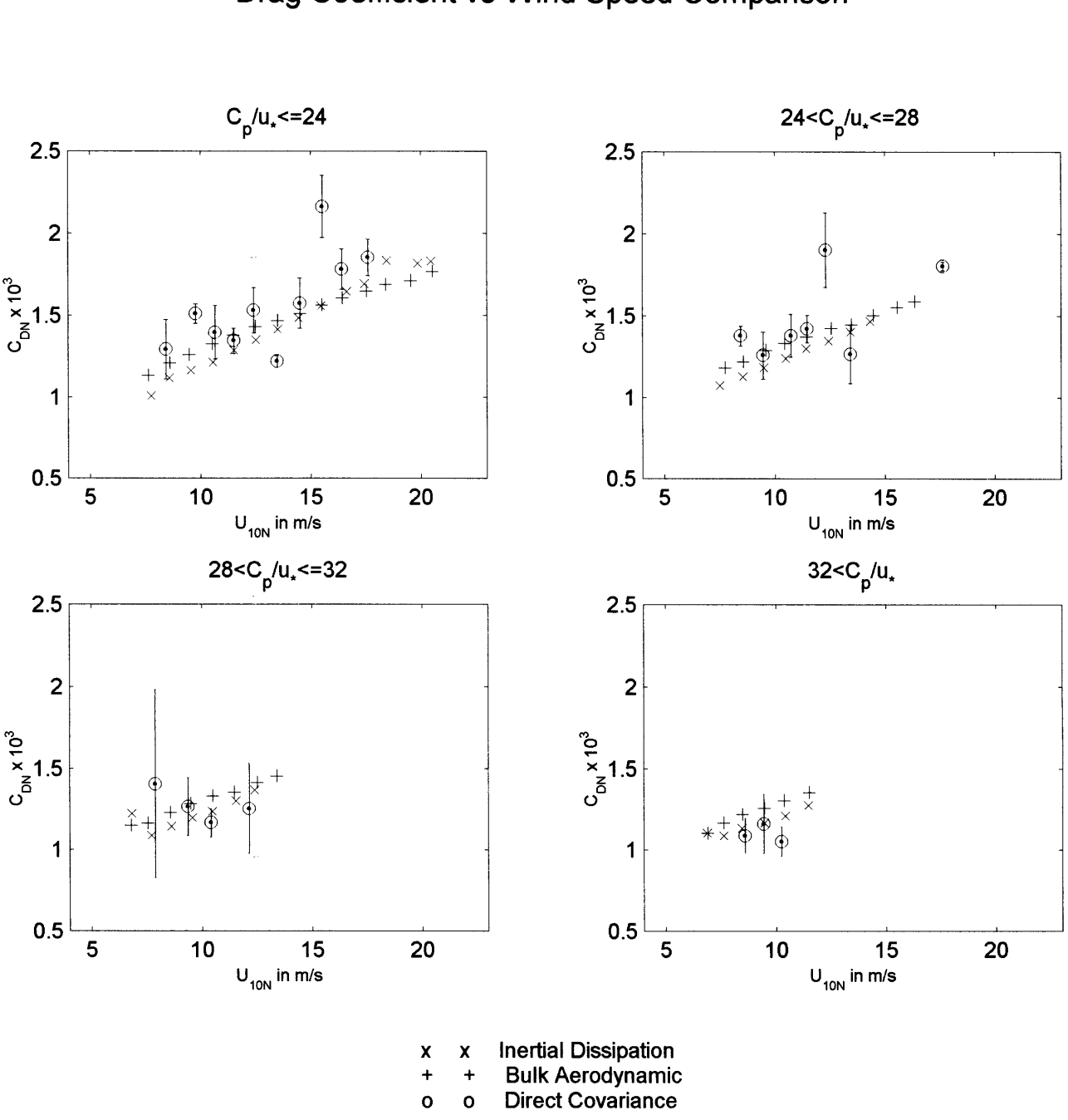

Figure 5.4 A comparison of the neutral drag coefficient C_{DN} estimated using the bulk aerodynamic, inertial dissipation, and motion-corrected covariance methods (averaged in increments of $U_{10N} = 1\,\text{m/s}$) for four different wave-age $\frac{C_p}{u_*}$ bins. The error bars for the covariance measurements denote the standard error.

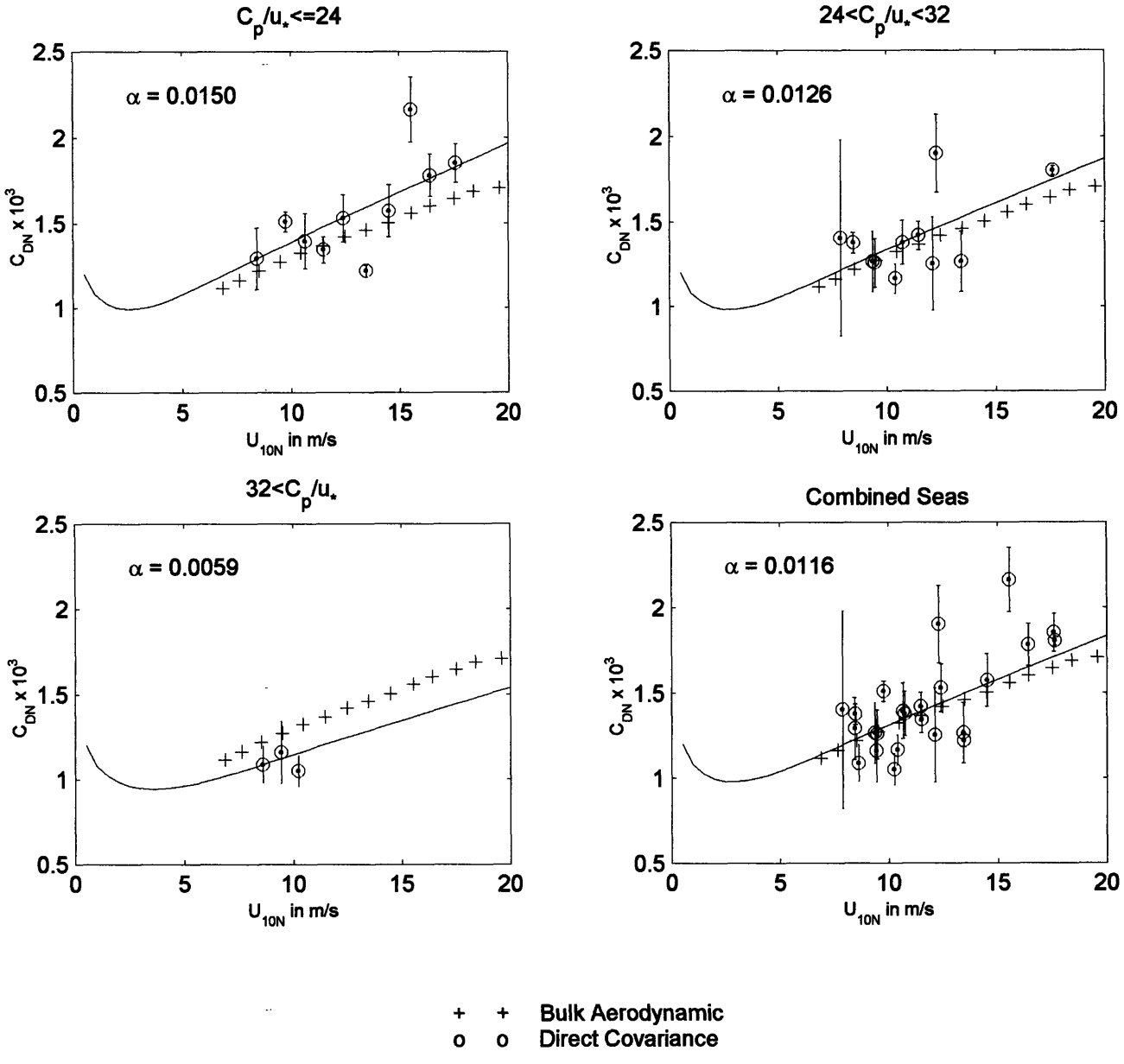

Figure 5.5 A comparison of the neutral drag coefficient, C_{DN}, estimated using the bulk aerodynamic method and compared to measurements obtained by the direct covariance method for four different wave-age bins. For each wave-age, the solid curves represent the best fit using Charnock's relation, $z_r = \frac{\alpha_c u_*^2}{g}$, where α_c represents the obtained Charnock's "constant" for each wave-age category. The data have been bin averaged in increments of $U_{10N} = 1\,\text{m/s}$, and the error bars for the covariance measurements denote the standard error.

Tropical Ocean-Global Atmosphere Coupled-Ocean Atmosphere Response Experiment (TOGA-COARE). The results obtained here imply that the drag coefficient is inversely correlated with wave-age; *i.e.*, the drag is higher for young (developing) seas and lower for fully-developed seas. This result has been theorized by Janssen (1989) and supported by experiments in the field (*e.g.*, Smith, 1980; Large and Pond, 1981; Geernaert *et al.*, 1986, 1987, 1988; Davidson *et al.*, 1991; Maat *et al.*, 1991; Smith *et al.*, 1992; Donelan *et al.*, 1993). Furthermore, this result supports the hypothesis that a roughness length computation (and, hence, drag coefficient) which includes characteristics of the wave field would provide improved bulk aerodynamic momentum flux estimates.

Like the bulk aerodynamic values, the neutral drag coefficients estimated by the inertial dissipation method do not exhibit a sea state dependence. For any given wind speed, C_{DN} is approximately the same value regardless of the wave-age. The inertial dissipation estimates, however, display a different trend than the bulk values when compared to the direct covariance measurements: the inertial dissipation values underestimate the actual drag for the youngest seas, but become progressively more accurate as the seas become fully-developed. This implies that the inertial dissipation method experiences the most error when estimating the momentum flux over the youngest seas, but that its performance improves with wave-age. As with the bulk aerodynamic method, these results suggest that incorporating sea-state dependence into the parameterizations used in the inertial dissipation model would improve momentum flux estimates.

5.3. PROPOSED INERTIAL DISSIPATION METHOD

The hypothesis that the dissipation profiles are influenced by wave-induced flow near the ocean surface implies that MO-similarity must break down in the wave boundary layer. This hypothesis can be investigated by comparing the vertical profiles of the dissipation rate with their MO-similarity prediction

$$\varepsilon_p = \frac{u_*^3}{\kappa z}\phi_\varepsilon(\zeta) \tag{5.1}$$

where $\zeta = z/L$ and we use the form of the dimensionless dissipation function given by Edson and Fairall (1998)

$$\phi_\varepsilon(\zeta) = \frac{(1-\zeta)}{(1-7\zeta)} - \zeta \qquad \zeta < 0 \tag{5.2a}$$

$$\phi_\varepsilon(\zeta) = 1 + 5\zeta \qquad \zeta > 0 \tag{5.2b}$$

Equation (5.1) is expected to over predict our dissipation estimates as long as there is a net flux of energy into the ocean. Evidence for this is shown in Figure 5.6, which illustrates that the measured dissipation profiles are less than their MO-similarity prediction. These measurements are averaged over a 2-hour period of increasing winds when the atmosphere was providing energy to growing (*i.e.*, young) seas. They were taken during the Office of Naval Research Marine Boundary Layers (MBL) experiment aboard the R/P FLIP (Edson *et al.*, 1997). The data collected from the FLIP mast allows us to compute all the terms of the total kinetic energy flux at three levels and the dissipation rate of KE at four levels.

The effect of the waves on the surface energy budget can be quantified by examining the ratio of the predicted to measured dissipation rate, $\frac{\varepsilon}{\varepsilon_p}$, as a function of sea state. The

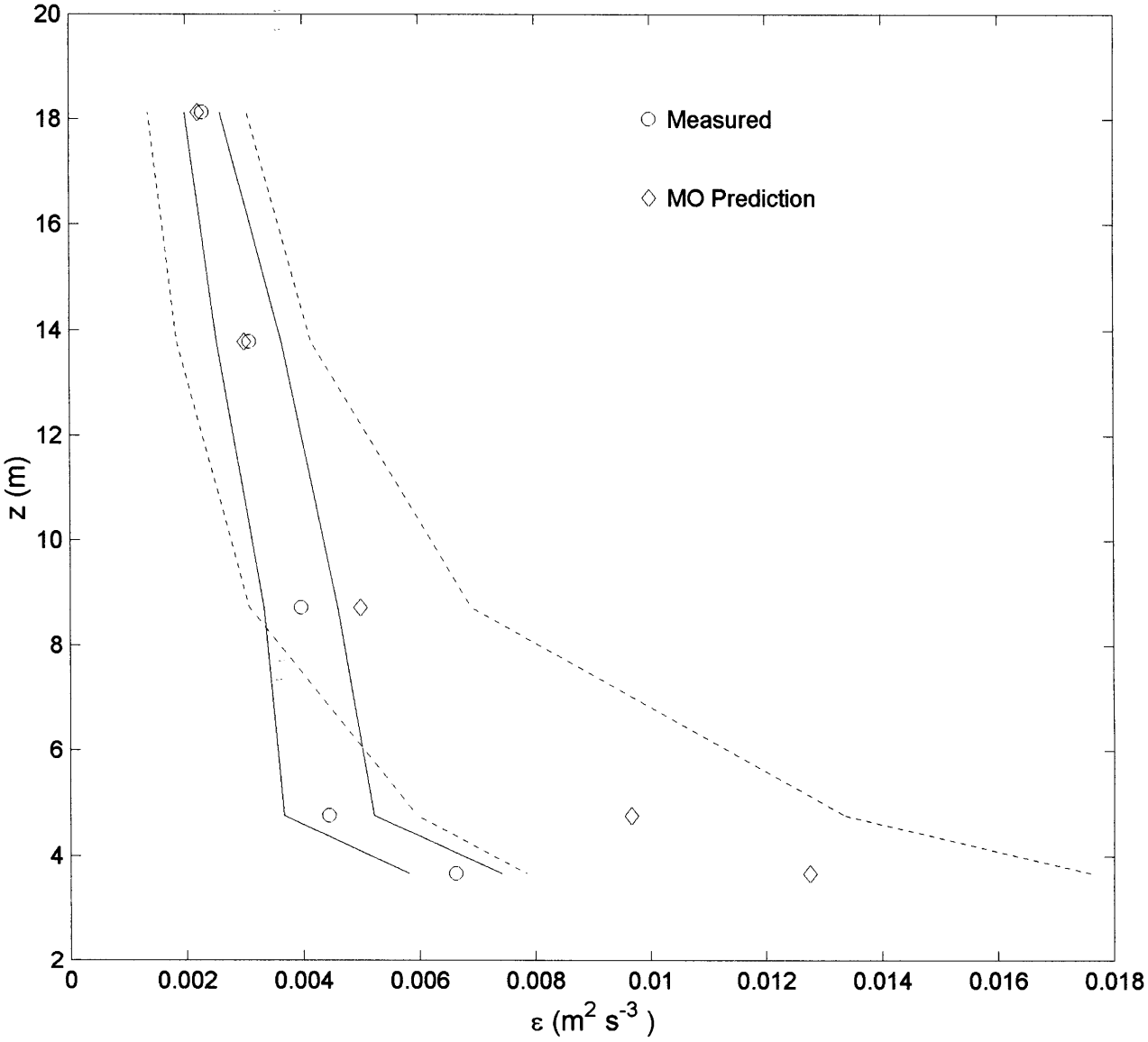

Figure 5.6 Dissipation measurements as a function of height taken during the ONR's Marine Boundary Layer (MBL) experiment aboard the R/P FLIP compared to their Monin-Obukhov similarity prediction. The solid and dashed curves represent the limits of the standard error of the measured and predicted values, respectively.

energy input into the ocean is investigated by bin averaging the ratio $\frac{\varepsilon}{\varepsilon_p}$ by the wave-age parameter, $\frac{C_p}{u_*}$. This allows examination of the dissipation profiles over developing, fully-developed, and decaying seas. The decay of the wave-induced effects as a function of sea-state is accounted for by multiplying the height of each measurement by the wavenumber of the dominant wave, k.

These bin-average estimates of $\frac{\varepsilon}{\varepsilon_p}$ are plotted versus the non-dimensional height kz in Figure 5.7. The lowest values of $\frac{C_p}{u_*}$ represents the youngest seas. The second and third bins span those wave-ages that are normally associated with fully-developed seas. The remaining ranges correspond to decaying conditions. These results indicate that there is an appreciable difference between the dissipation estimates and their MO-similarity predictions for all sea-states when $kz < 1$. The results indicate that the deficit is greatest over the youngest seas and decreases with increasing wave age, a conclusion that is also supported by the drag coefficient computations which indicated increasing accuracy of the inertial dissipation method as the seas become fully-developed. This supports the hypothesis that the dissipation deficit is a function of sea state and clearly shows that the dissipation rates do not obey MO-similarity in the wave boundary layer. The results also indicate that MO-similarity is again valid above the wave boundary layer at heights corresponding to $kz > 1.5$.

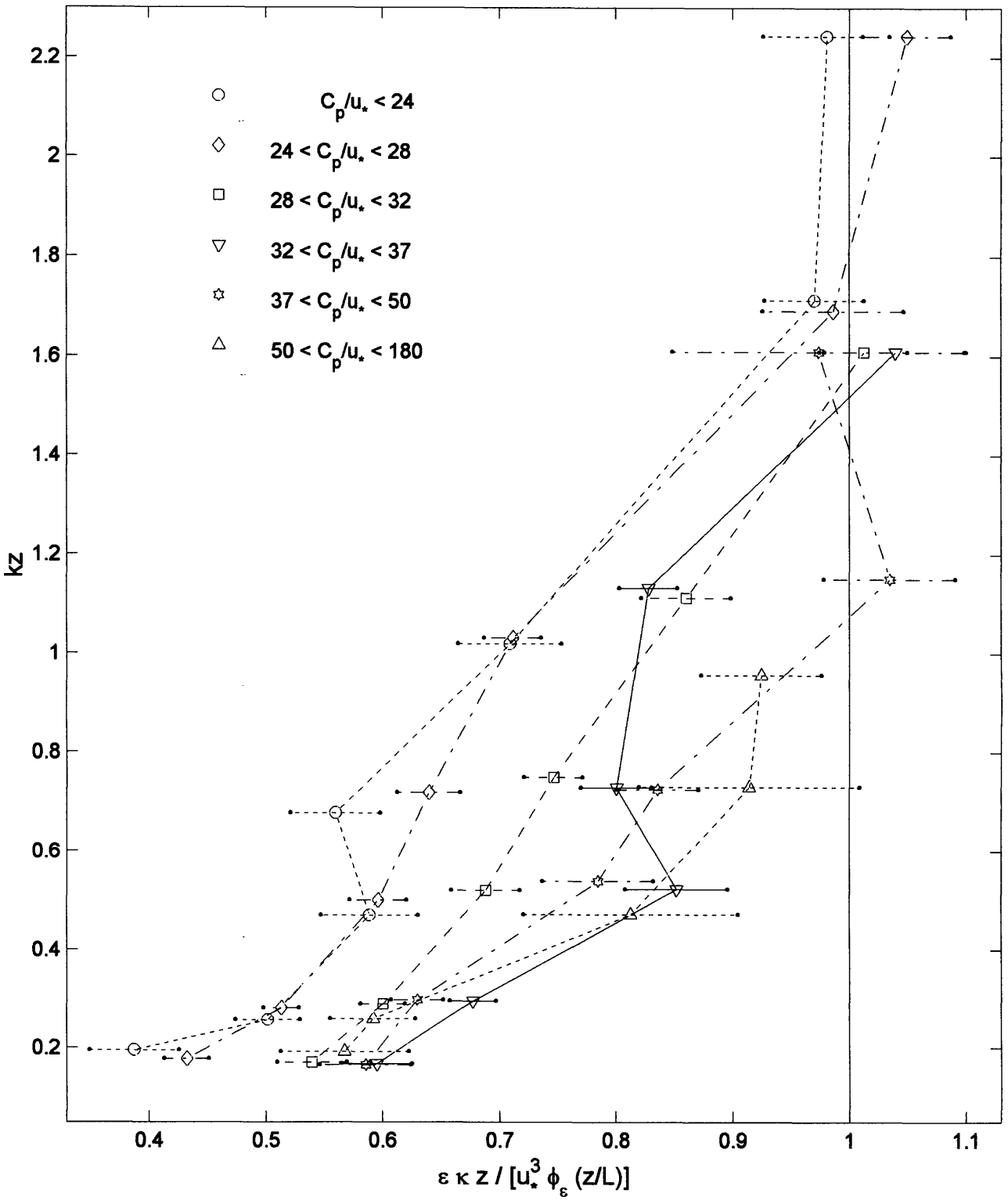

Figure 5.7 Ratio of predicted to measured dissipation rates versus non-dimensional height for six wave-age bins. Symbols: o- - - $C_p/u_* < 24$; ◇—— $24 \le C_p/u_* < 28$; □—— $28 \le C_p/u_* < 32$; ▽—— $32 \le C_p/u_* < 37$; ☆—— $37 \le C_p/u_* < 50$; and △- - - $50 \le C_p/u_* < 180$. The error bars denote the standard error for each measurement.

Application of the inertial dissipation method to over ocean measurements therefore requires modification to equation (5.1) to account for the wave-induced effects. A simple means to accomplish this involves fitting curves to the dimensionless profiles shown in Figure 5.7 as

$$\frac{\varepsilon \kappa z}{u_*^3} = 1 - f\left(\frac{C_p}{u_*}, kz\right) \tag{5.3}$$

where the function, f, includes the effects of the waves on the production and transport terms. Clearly, the function should decay to zero above the wave boundary layer. Its behavior near the surface is much less obvious. However, some insight into its behavior is gained by considering the surface energy flux, $F(0)$, which is continuous across the interface. Therefore, the vertical derivative of this flux, which is closely related to the energy budget and ε, must approach zero very near the surface. A simple function that meets these upper and lower constraints while closely fitting the measurements as shown in Figure 5.8 is given by

$$f\left(\frac{C_p}{u_*}, kz\right) = \frac{30u_*}{C_p}(2kz)e^{-2kz} \tag{5.4}$$

This function is used to correct the CMO dissipation estimates in the following analysis such that the proposed dimensionless dissipation function is now given by

$$\phi_{\varepsilon_m} = \phi_\varepsilon\left(1 - \frac{30u_*}{C_p}(2kz)e^{-2kz}\right) \tag{5.5}$$

where ϕ_ε is calculated using equations 5.2(a) and 5.2(b).

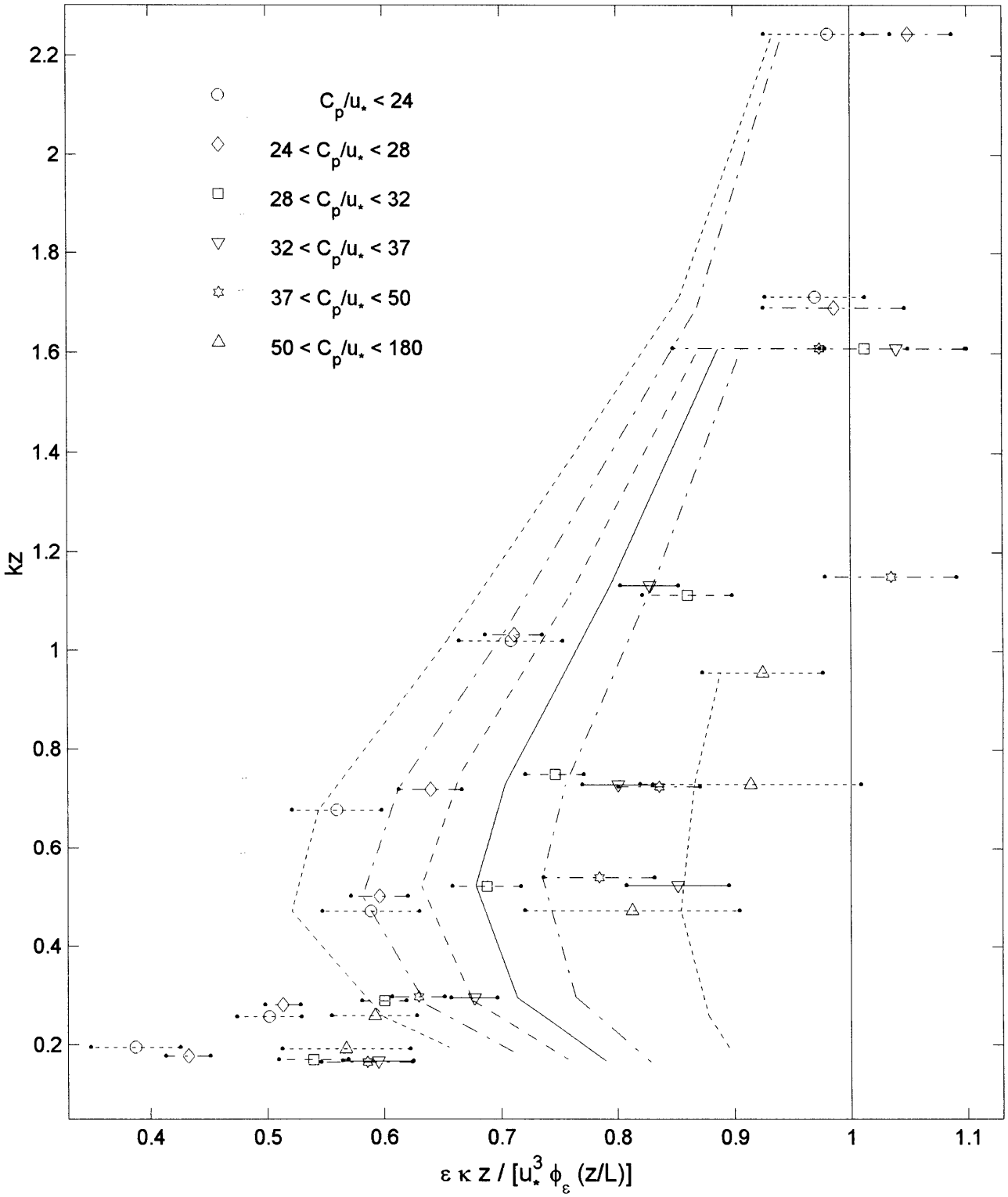

Figure 5.8 Ratio of predicted to measured dissipation rates versus non-dimensional height for six wave-age bins. The curves represent the function $f = \frac{30u_*}{C_p}(2kz)e^{-2kz}$ and the error bars denote the standard error. The symbols are the same as in Figure 5.7.

The modified inertial dissipation estimates are compared to the original dissipation estimates and the direct covariance measurements of the friction velocity in Figure 5.9. Whereas the previous inertial dissipation method systematically under predicted the momentum flux, the new parameterization improves the estimates substantially. The mean deviation of the inertial dissipation values calculated from the previous model was 0.049 m/s. The estimates calculated from the proposed inertial dissipation method deviate by one-third the previous error; *i.e.*, the mean deviation is only 0.032 m/s. Thus, employing the new parameterization results in over a 33% reduction in the error associated with calculating friction velocity estimates using the inertial dissipation method.

Importantly, the new parameterization, ϕ_{ε_m}, was developed using an independent data set measured over open-ocean conditions of unlimited fetch and depth. This suggests the universality of the modified function and serves as satisfactory validation of the parameterization. That is, the parameterization has not been "tuned" to fit the CMO measurements, but rather was developed independently and found to result in impressive improvement of the dissipation method when compared to the motion-corrected direct covariance measurements.

5.4. Modified Bulk Aerodynamic Methods

The approach proposed in this section is based upon the ideas, presented in section 4.2.2, that Charnock's expression for the surface roughness, z_r, accounts for the roughness of the short gravity-capillary waves. However, modifications of the drag due to gravity waves and swell are not included in standard bulk formula. To improve drag coefficient estimates and, therefore, wind stress estimates in the bulk aerodynamic model,

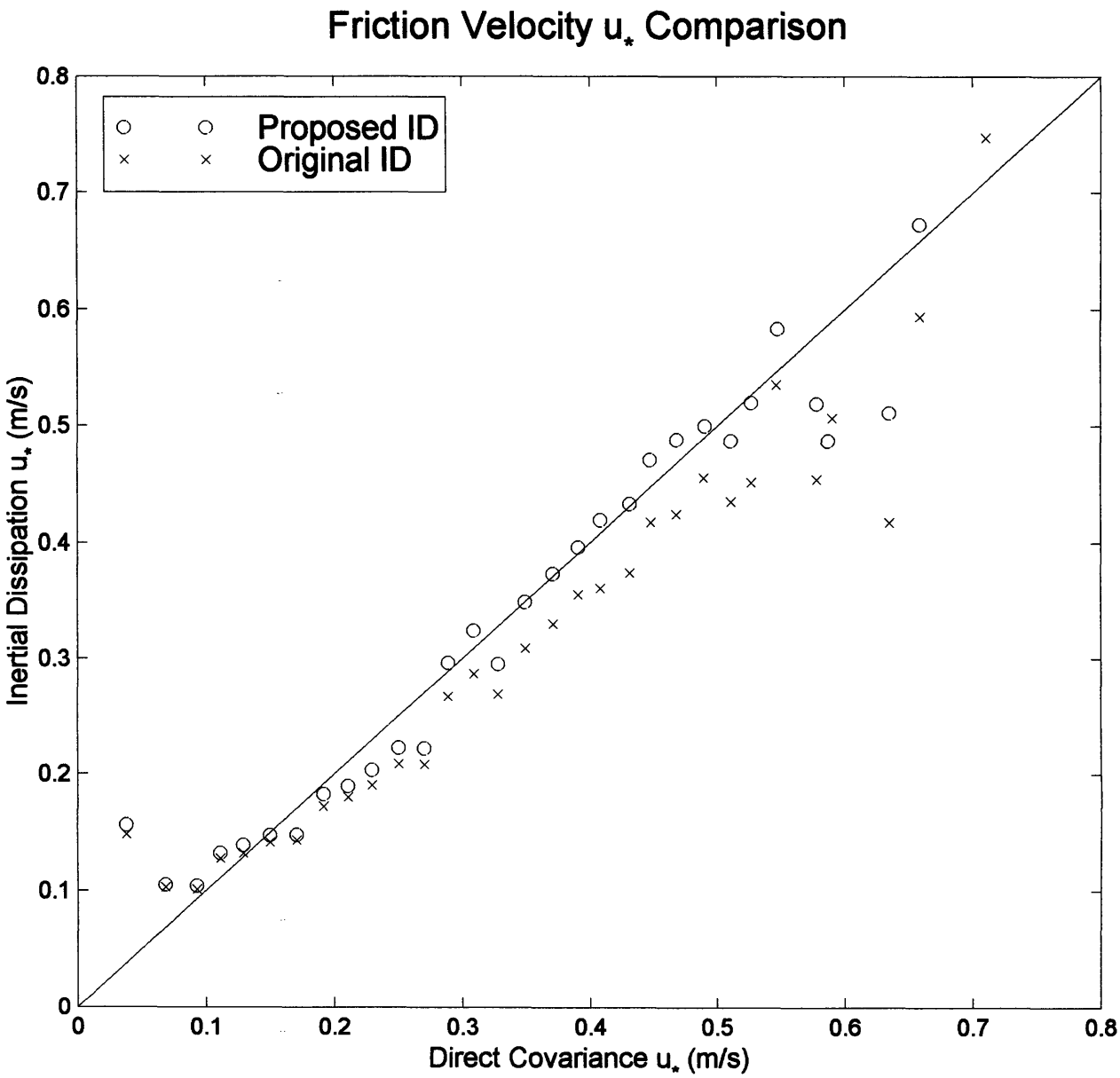

Figure 5.9 Friction velocity, u_*, comparison for original and proposed inertial dissipation methods and direct covariance method. Symbols: o Proposed inertial dissipation method; × Original inertial dissipation method. Data are bin averaged in increments of 0.02 m/s.

we need to relate the total drag (short plus long waves) to wave parameters in a quantitative manner.

The goal of directly relating the sea surface drag coefficient to sea state has remained elusive (Smith *et al.*, 1992; Dobson *et al.*, 1994). Donelan (1982) was one of the first to present field data which showed a strong relationship between wave parameters and wind stress. His research demonstrated the breakdown of Charnock's relation between the aerodynamic roughness length and the friction velocity in all but fully-developed wave conditions.

Since this pioneering work, other researchers have attempted to define a quantitative relationship between the wind and wave fields. Smith (1991) demonstrated a "drag coefficient anomaly," a departure of the drag coefficient from values expected through the use of Charnock's expression, which was significantly correlated with wave age:

$$10^3 \Delta C_{DN} = 1.85 - 2.24 \frac{C_p}{(U_{10N} \cos\theta)} \tag{5.5}$$

where C_p and U_{10N} are expressed in ms^{-1} and θ is the difference between the wind and wave directions. Geernaert *et al.* (1986) proposed an empirical relation between wind stress and wave age; however, lacking wave spectral data, they were forced to estimate the wave field from wind data and may have predetermined their results on account of this circular argument. Following the ideas of Kitaigorodskii (1973) and Janssen (1989), Nordeng (1991) proposed a "wave age dependent Charnock constant":

$$\alpha_c = z_* = \frac{g z_r}{u_*^2} = f\left(\frac{C_p}{u_*}\right) \tag{5.6}$$

However, this approach cannot convincingly stand alone since u_* appears in both z_* and the wave age, and self-correlation may produce spurious results (Hicks, 1978; Dobson *et al.*, 1994).

5.4.1. Scaling Roughness Length with Wave Amplitude

An alternate approach, which is explored here, is derived from Donelan *et al.* (1993). The aerodynamic roughness length is scaled by the rms amplitude σ of the waves, where σ is defined in terms of the significant wave height, H, as $4\sigma = H$ and where $\frac{z_r}{\sigma}$ expresses the ability of the waves to serve as roughness elements (Donelan, 1990). The benefit of regressing the ratio of $\frac{z_r}{\sigma}$ to inverse wave age is that the dimensionless ratios are formed from four independent parameters, and the regression avoids the problem of self-correlation by estimating the sea surface roughness from wave age parameters (σ and C_p) that can be measured *in situ* (Smith *et al.*, 1992).

Since the idea that the roughness length should be correlated with the height of the waves depends on the concept of rough aerodynamic flow, attention is limited to cases for which $U_{10} > 7.5\,\text{m/s}$ (Wu, 1980; Donelan, 1990). Thus, the following roughness length determination applies only to fully rough flow. This formulation does not apply to cases for which the surface layer appears to be aerodynamically smooth, $U_{10} < 3\,\text{m/s}$, or to transitional flow.

As depicted in Figure 5.10, inverse wave-age estimates from the modified inertial dissipation method exhibit an increase of roughness scaled with rms wave height, as expressed quantitatively by the regression line

$$\frac{z_r}{\sigma} = 9.6\times10^{-4}\left[\frac{U_{10N}}{C_p}\right]^{2.7} \tag{5.7}$$

which displays good agreement to the regression line

$$\frac{z_r}{\sigma} = 5.5\times10^{-4}\left[\frac{U_{10N}}{C_p}\right]^{2.7} \tag{5.8}$$

fitted to data obtained in 12 m of water on Lake Ontario (Donelan *et al.*, 1993) and agrees well to the $\left[(U_{10N}/C_p)^{3.5}\right]$ power law obtained by Smith *et al.* (1992) from data obtained during the Humidity Exchange over the Sea (HEXOS) experiment in 18 m of water over the North Sea. In contrast, Dobson *et al.* (1994) found a weaker $\left[(U_{10N}/C_p)^{1.7}\right]$ power law for data obtained during the Grand Banks ERS-1 SAR Wave Validation Experiment. However, the scatter in their data set did not allow them to resolve the slope (power law) well, and they indicate that a neutral or two way regression would give a steeper $\left[(U_{10N}/C_p)^{3.5}\right]$ power law, which would be in better agreement with the power laws obtained using the CMO, Lake Ontario, and North Sea data sets. The close agreement in the power laws obtained in four independent experiments, which ranged in environmental conditions from lake to open ocean, suggests the strength of the relationship between the surface roughness length, the rms height of the dominant seas and the wave age, as expressed in equation (5.7).

In Figure 5.11, the CMO rms wave height measurements are empirically related to the wave age and wind speed by the regression line

$$\frac{\sigma^2 g^2}{(U\cos\theta)^4} = 2.9\times10^{-3}\left[\frac{U_{10N}}{C_p}\right]^{-1.8} \tag{5.9}$$

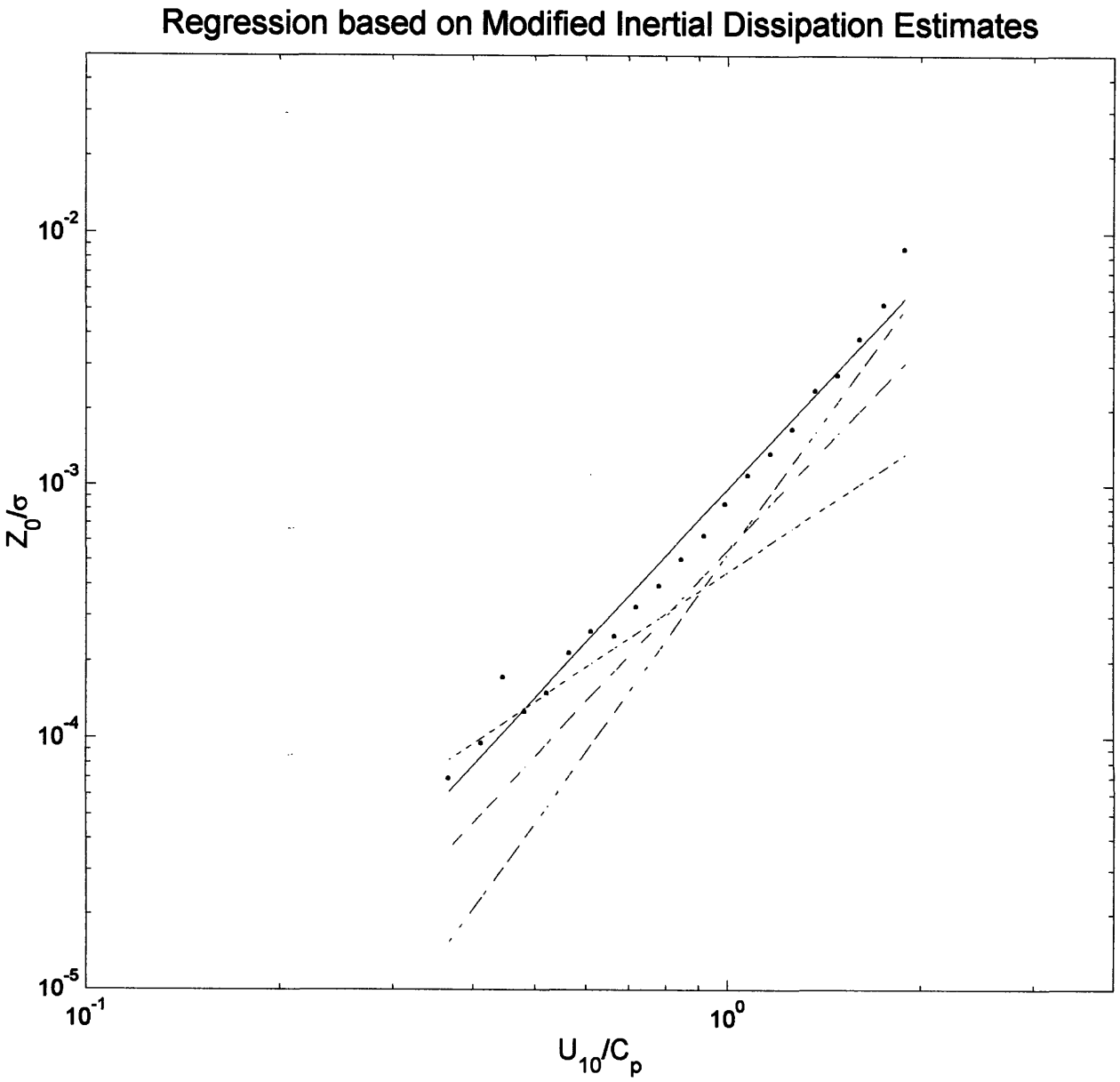

Figure 5.10 The ratio of measured roughness length z_r to rms wave height σ versus inverse wave age U_{10}/C_p, binned in increments of log(0.035). Symbols: • CMO data; — regression on present data, equation (5.7); --- Dobson *et al.* (1994); — – Donelan *et al.* (1993), equation (5.8); — – – – Smith *et al.* (1992).

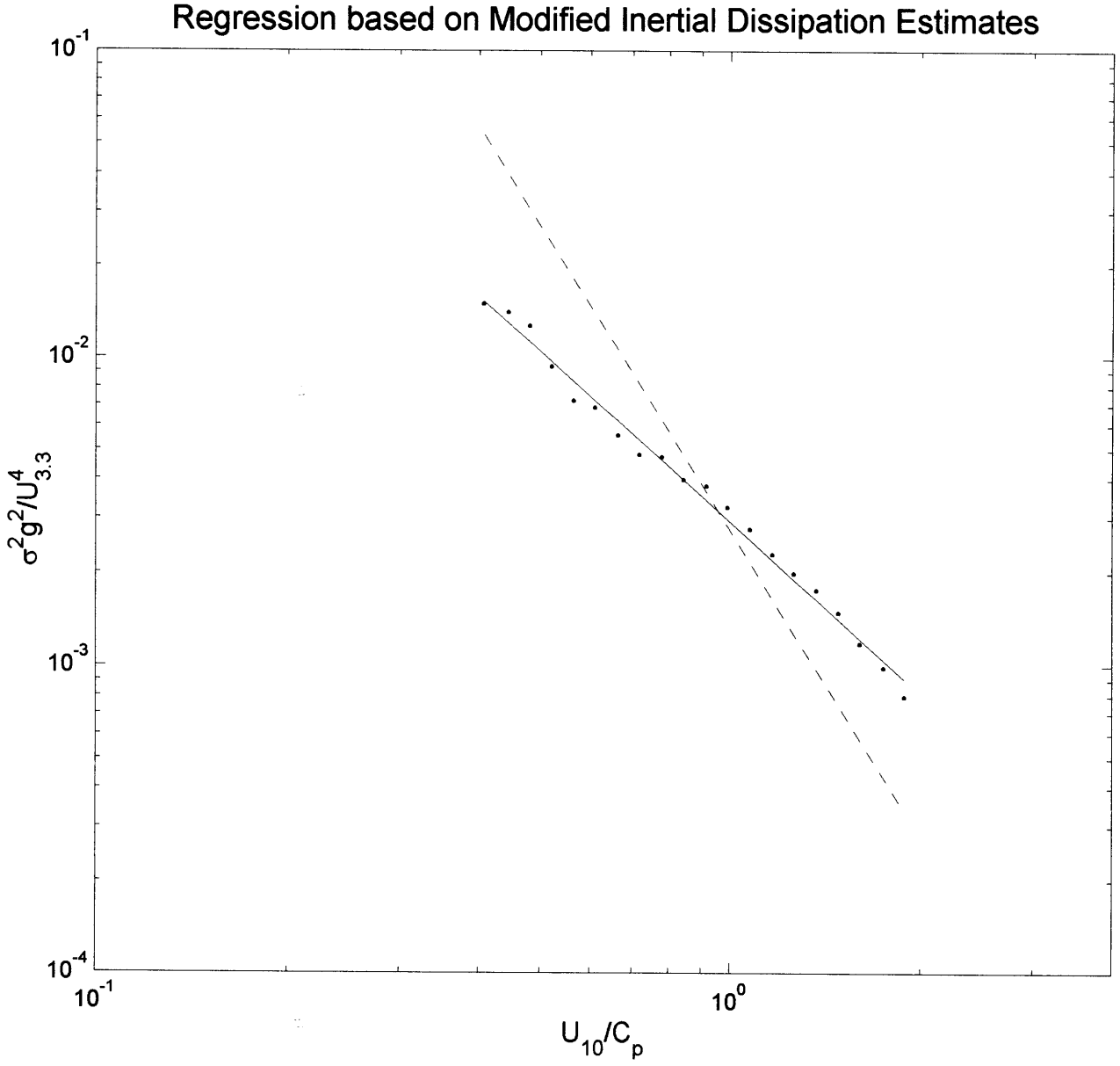

Figure 5.11 The ratio of the square of rms wave height σ^2 times the square of gravity g^2 versus inverse wave age U_{10N}/C_p, binned in increments of $\log_{10}(0.035)$.
Symbols: •• CMO data; —— regression on present data, equation (5.9); — —Donelan *et al.* (1985).

where g is the acceleration of gravity and θ is the angle between the winds and the waves. Donelan *et al.* (1985) found a steeper $\left[\left(U_{10N}/C_p\right)^{-3.3}\right]$ relationship using their Lake Ontario field data. Examination of Figure 5.11 reveals that the regression used to obtain equation (5.9) is a relatively tight fit. The marked difference between the power laws derived from the Lake Ontario and CMO data sets is a reflection of the different environmental regimes, the data from Donelan *et al.* (1985) representing shallow lake conditions and our data representing ocean conditions over the continental shelf. These differences can include, for example, a dependence on fetch that is felt at the lake site but not at the CMO site.

Assuming that the wind and wave fields are aligned at the surface $(\cos\theta \approx 1)$, equation (5.9) may be simplified

$$\sigma = 5.4\times10^{-2}\left[\frac{U^2}{g}\right]\left[\frac{U_{10N}}{C_p}\right]^{-0.92} \tag{5.10}$$

Substituting the expression for the rms wave height, equation (5.11), into equation (5.7) provides an expression for the roughness length

$$z_r = 5.2\times10^{-5}\left[\frac{U^2}{g}\right]\left[\frac{U_{10N}}{C_p}\right]^{1.8} \tag{5.11}$$

which has a steeper power law than the expression derived by Donelan *et al.* (1993)

$$z_r = 3.7\times10^{-5}\left[\frac{U^2}{g}\right]\left[\frac{U_{10N}}{C_p}\right]^{0.9} \tag{5.12}$$

due to the different empirical relationship for the dependence of the wave height on wind speed. Equation (5.11) implies that the roughness length depends quadratically on the

wind and wave-age. However, as mentioned, this relationship for the roughness length is only applicable to the same type of ocean conditions present at the CMO site because the parameterizations do not give the same rms wave height, σ, for the same wind speed and wave age. This severely limits the widespread application of this type of parameterization. Thus, it is preferable to return to equation (5.7) which appears to be a more robust relationship since the scaling gives similar results under similar conditions at all sites.

Equation (5.7) is now used in the bulk aerodynamic method as an alternate means of calculating the roughness length. It was hypothesized that including sea state dependence into drag coefficient calculations would improve the wind stress estimates, particularly in the case of young (developing) seas. Friction velocity estimates calculated by the modified bulk method are depicted in Figure 5.12. Overall, the new parameterization slightly improves the u_* estimates when compared to their former values, although the difference is not statistically significant. Of note, the modified bulk method results in higher friction velocity estimates than the original method for all wind speeds $u_* > 0.2$ m/s, and the new parameterization produces estimates that over predict the actual momentum flux for $u_* > 0.3$ m/s. Although statistically the modified bulk aerodynamic method yields the same error as the original method, the trend is significantly different. Whereas the original method tended to over predict the momentum flux over decaying seas and underestimate the flux over developing seas, the modified method tends to over predict the flux for all wave ages, which suggest that there is an inherent bias in the correction.

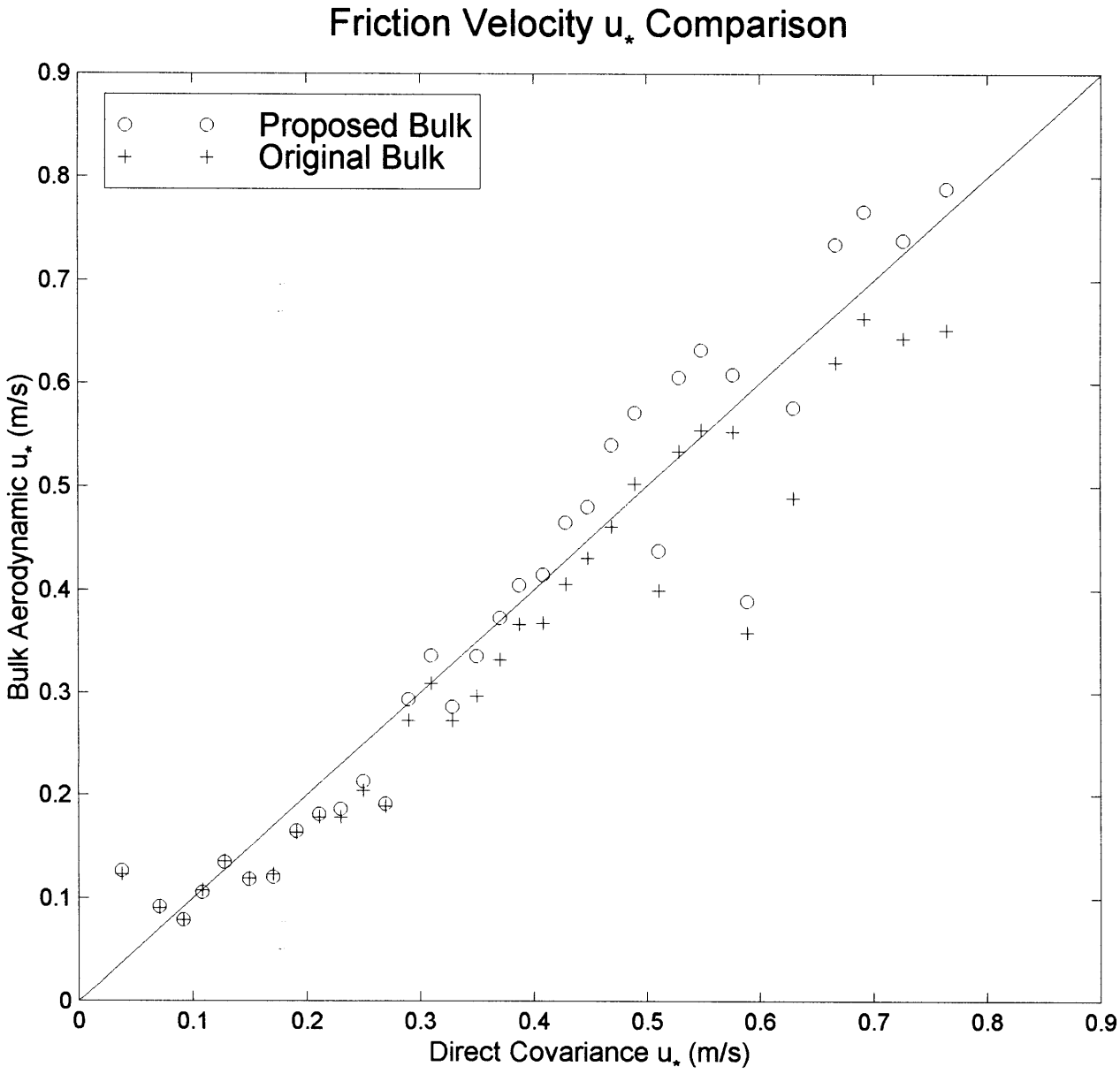

Figure 5.12 Friction velocity, u_*, comparisons of the bulk aerodynamic versus motion-corrected covariance method for the original bulk method (+) and the modified parameterization (o). Values of u_* are bin-averaged in increments of 0.02 m/s.

One limitation of this model is the log-linear regression required by equation (5.7). A closer inspection of Figure 5.11 reveals that the points indicate that either a curve or two different linear regressions would more adequately estimate $\frac{z_r}{\sigma}$. Additionally, notice that the young seas, $\left(\frac{U_{10N}}{C_p} \approx 1\right)$, only represent about 10% of the total data, yet tend to increase the slope (power law) significantly. In fact, when only the young data is considered, the power law increases to $\left[\left(U_{10N}/C_p\right)^{-3.0}\right]$, whereas if only the fully-developed and decaying seas are considered, the slope decreases to $\left[\left(U_{10N}/C_p\right)^{-2.0}\right]$. Notice that these results are within the span of ranges found by other researchers (Smith *et al.*, 1992; Donelan *et al.*, 1993;; Dobson *et al.*, 1994) and could, in part, explain the differences that are found.

In Figure 5.13, the new bulk aerodynamic estimates are compared to direct covariance drag coefficient measurements. In contrast to the bulk estimates in Figure 5.4, the modified roughness length calculation results in sea state dependent drag coefficients; for a given wind speed, the predicted drag coefficient is inversely related to wave-age. However, the tendency of the $\left[\left(U_{10N}/C_p\right)^{-2.7}\right]$ power law to overestimate the friction velocity results in higher than expected drag coefficients for all wave ages and wind speeds.

5.4.2. Modified Charnock's Relation

The overall goal is to provide the best momentum flux estimates for the Coastal Mixing and Optics experiment. While the results obtained using the approach of Donelan *et al.* (1993) are promising, the new estimates are not significantly improved over the

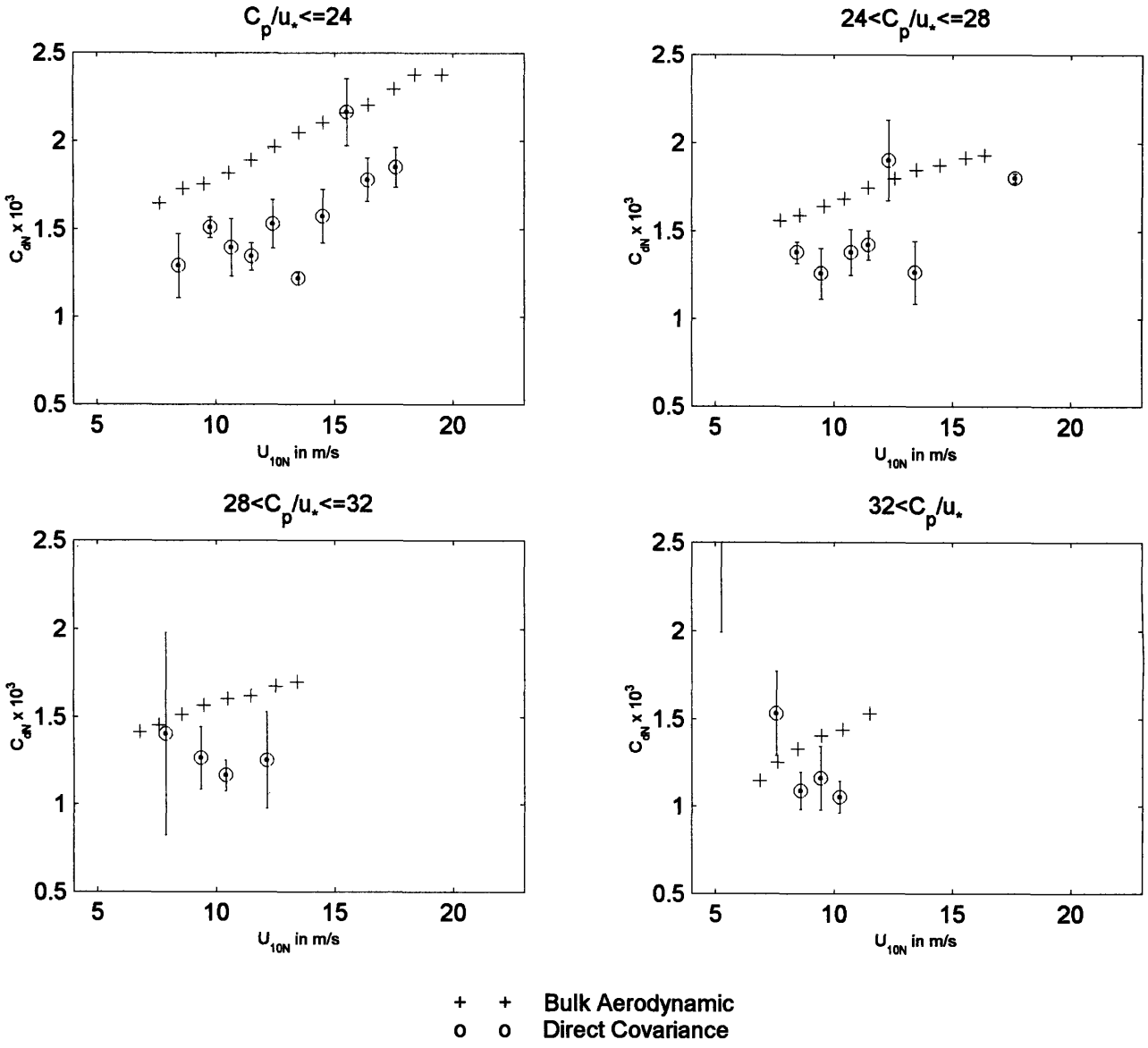

Figure 5.13 A comparison of the neutral drag coefficient C_{DN} estimated using the modified bulk aerodynamic method and compared to motion-corrected covariance measurements (averaged in increments of 1 m/s) for four different wave-age $\frac{C_p}{u_*}$ bins. The error bars for the covariance measurements denote the standard error.

previous values. Furthermore, the parameterization tends to overestimate the roughness length for all wind speeds, a trend which indicates an inherent bias in the model. Thus, still in pursuit of a means to reconcile the current deficiency of the bulk aerodynamic method to estimate the wind stress in cases of young (developing) seas, but not to overestimate the wind stress in cases of fully-developed or decaying seas, another method of forcing a wave-age dependence into the roughness length via the Charnock's "constant" is explored. On the basis of the direct covariance measurements, the Charnock's "constants" that provided the best fits for young, fully-developed, and decaying seas are $\alpha_c = 0.0150$, $\alpha_c = 0.0126$ and $\alpha_c = 0.0059$, respectively. Figure 5.14 shows the measured Charnock's parameter as a function of wave age, for which the function

$$\alpha_c = -4.05\times10^{-4}\left(\frac{C_p}{u_*}\right) + 2.34\times10^{-2} \tag{5.13}$$

provides the best linear regression. Revisiting equation (4.19), the approach of Smith (1988) is modified

$$z_0 = z_s + z_r \tag{5.14}$$

where z_s is determined as before [equation (4.20)], but z_r is now expressed as

$$z_r = \alpha_c \frac{u_*^2}{g}$$

where

$$\alpha_c = -4.05\times10^{-4}\left(\frac{C_p}{u_*}\right) + 2.34\times10^{-2} \qquad \text{for } \frac{C_p}{u_*} < 43 \tag{5.15}$$

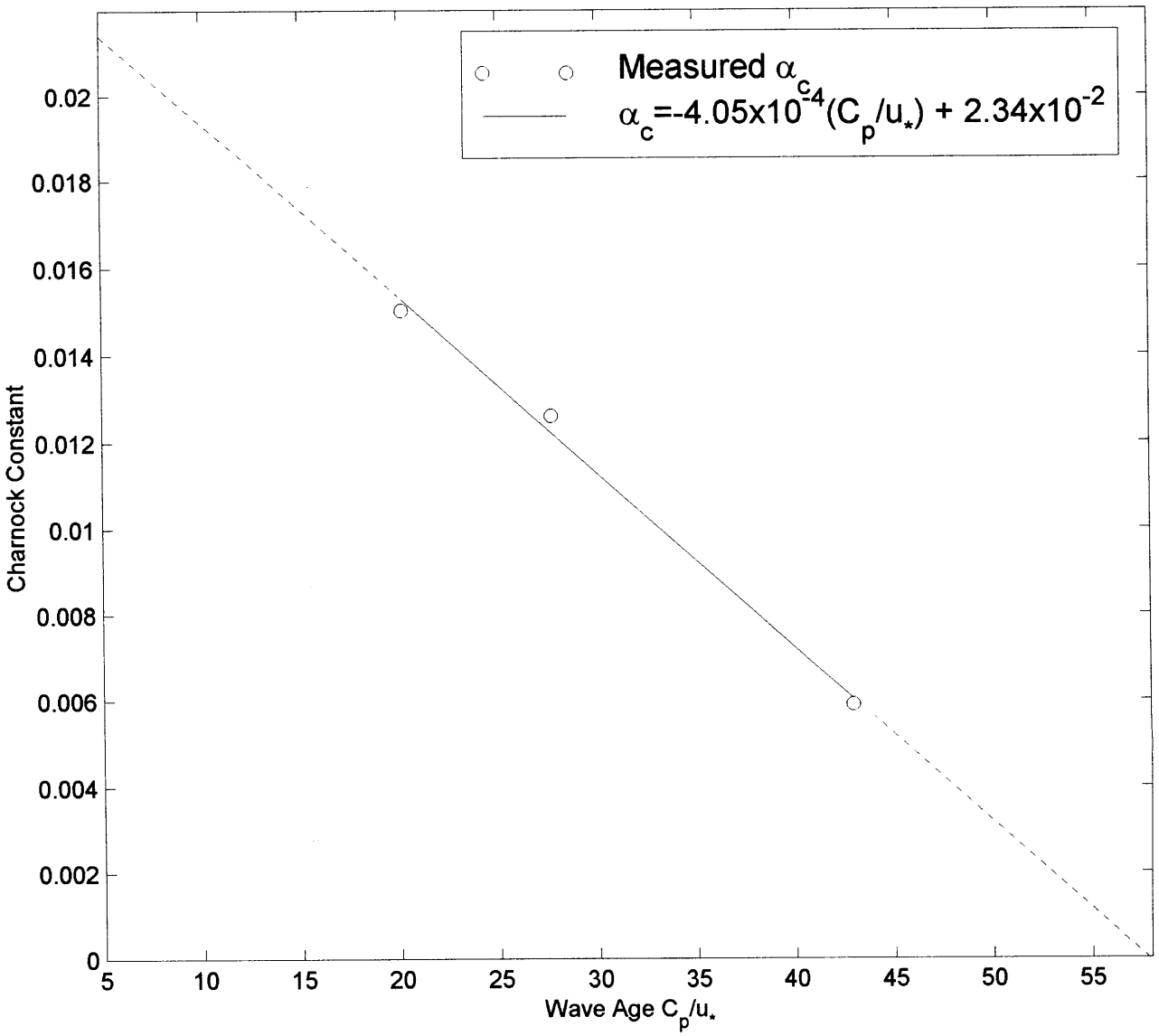

Figure 5.14 Estimated wave age dependent Charnock's "constant":

$$\alpha_c = -4.05\times10^{-4}\left(\frac{C_p}{u_*}\right) + 2.34\times10^{-2}.$$

For seas with wave ages older than $\frac{C_p}{u_*} \geq 43$, the Charnock's parameter is assigned the value of $\alpha_c = 0.0059$, the value of the upper limit.

The modified Charnock's parameterization results in improved friction velocity estimates, as illustrated in Figure 5.15. Whereas the original bulk estimates had a mean deviation of 0.046 m/s, the new parameterization reduces the error by 7% and results in a mean deviation of 0.043 m/s. While this may seem small, the subsequent improvement in the drag coefficient estimates (Figure 5.16) is quite noticeable. Previously, the bulk aerodynamic method underestimated the drag associated with young seas, but now the estimates are in good agreement with the direct covariance measurements. For the remaining three wave-age bins, the modified Charnock's expression again provides improved estimates of the drag over fully-developed and decaying seas. These results suggest that there is a benefit to incorporating wave-age dependence into the bulk aerodynamic model, even if the forcing is as simple as including a wave-age dependent Charnock's parameter. Obviously, further research is required to validate the function proposed here, especially since the wave-age span is limited: the youngest seas averaged $\frac{C_p}{u_*} \approx 20$, and the oldest seas averaged $\frac{C_p}{u_*} \approx 43$, providing a somewhat limited range upon which the proposed function is based. Thus, while the relationship proposed here improves the bulk aerodynamic momentum flux estimates for the CMO experiment, future studies are needed to validate or improve the parameterization. Most importantly, the results indicate that bulk aerodynamic momentum flux estimates can be improved by incorporating sea state dependence via a roughness length determination.

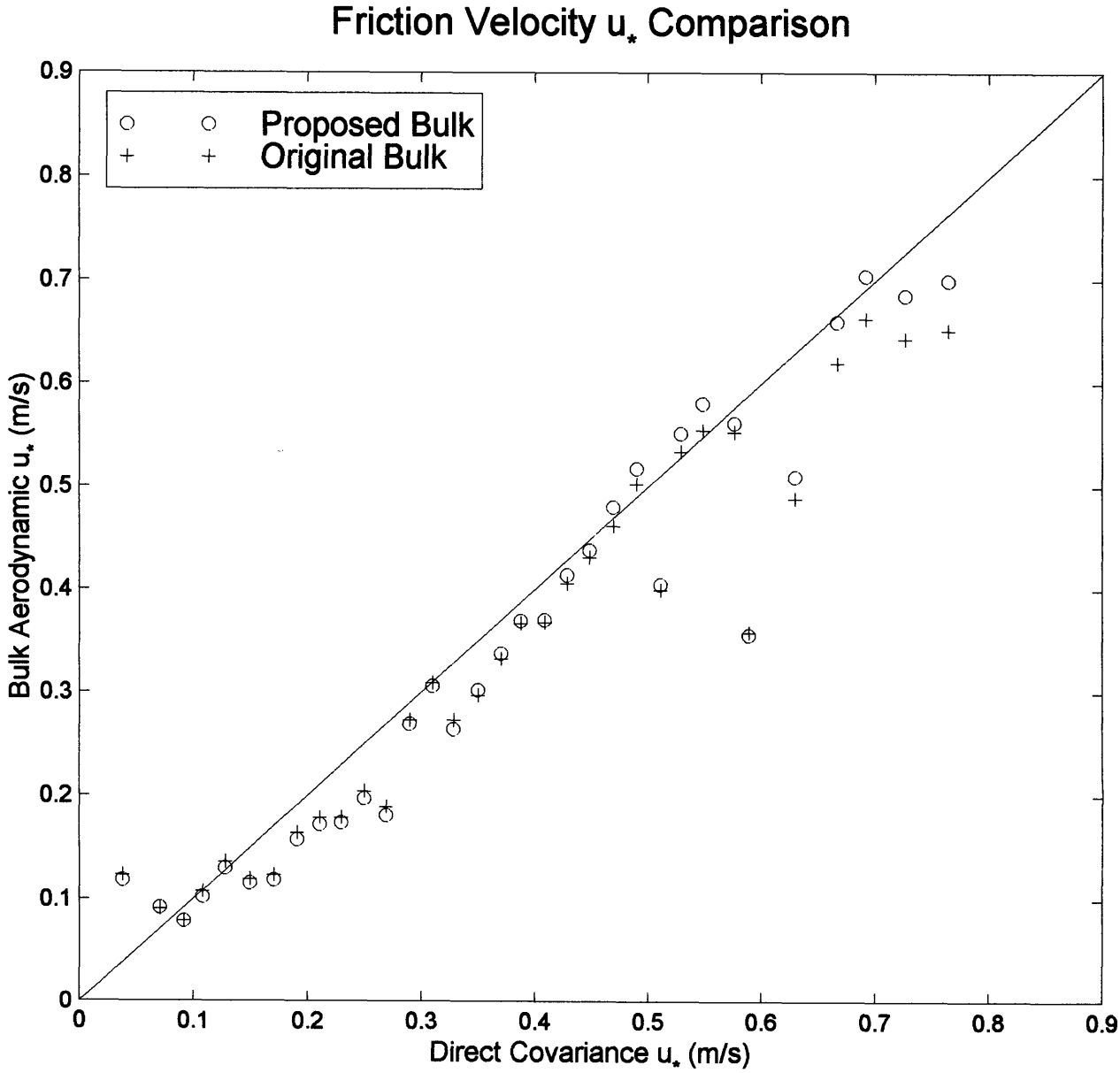

Figure 5.15 Friction velocity, u_*, comparisons of the bulk aerodynamic versus motion-corrected covariance method for the original bulk method (+) and the modified-Charnock parameterization (o). Values of u_* are bin-averaged in increments of 0.02 m/s.

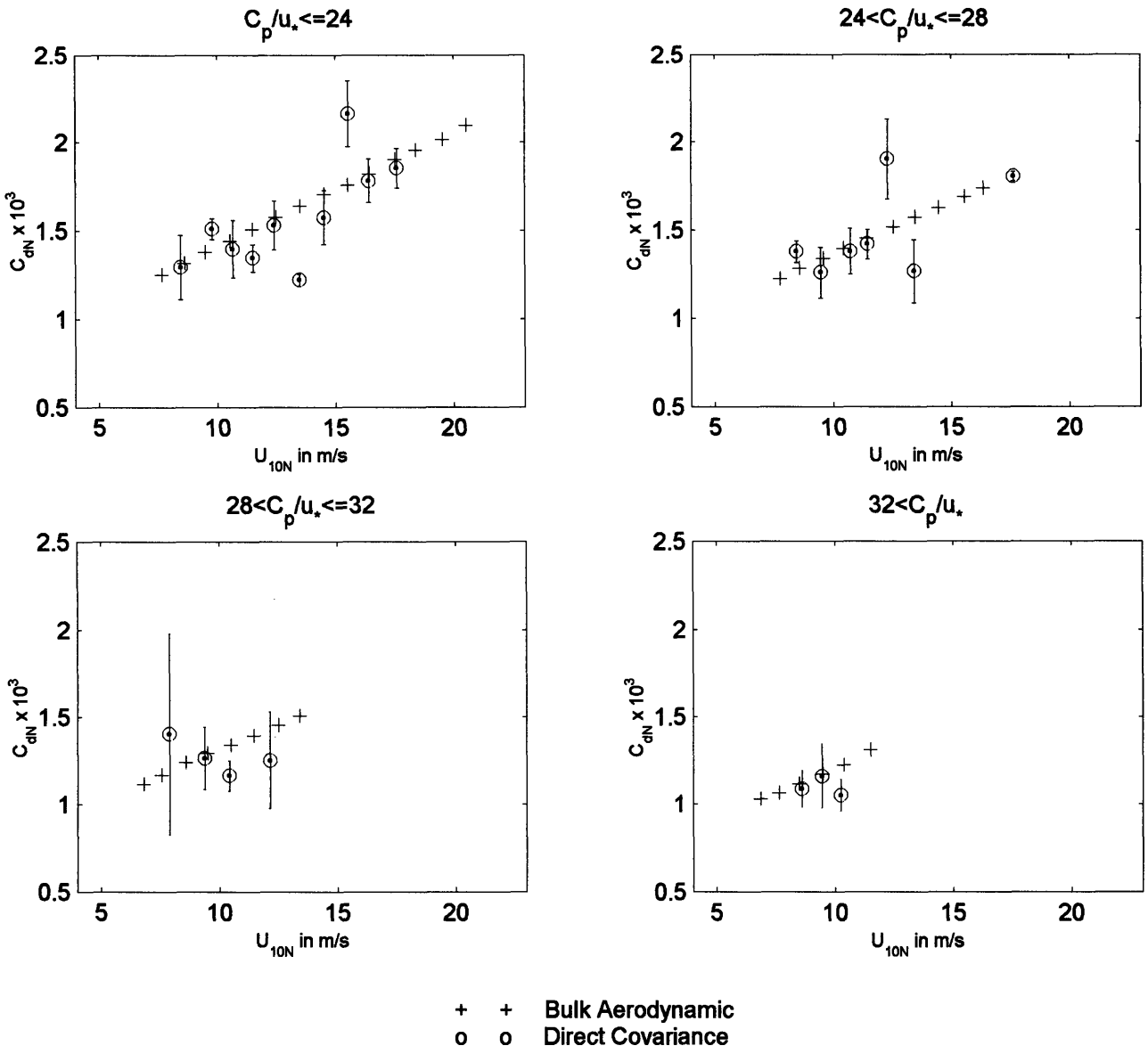

Figure 5.16 A comparison of the neutral drag coefficient C_{DN} estimated using the modified-Charnock bulk aerodynamic method and compared to motion-corrected covariance measurements (averaged in increments of 1 m/s) for four different wave-age $\frac{C_p}{u_*}$ bins. The error bars for the covariance measurements denote the standard error.

6. CONCLUSIONS

The work presented in this thesis is an investigation of the influence of surface waves on momentum exchange. Accurate measurements of the exchange of momentum and energy between the atmosphere and ocean are critical to numerical prediction systems. The growing sophistication of current numerical models, such as the United States Navy's Coupled Ocean Atmosphere Prediction System, requires an accurate representation of the dynamics and magnitude of energy transfer through the air-sea interface. This thesis explored the theoretical framework which forms the basis for the direct covariance (eddy correlation), direct / inertial dissipation and bulk aerodynamic methods for measuring and calculating momentum flux. Unlike the other methods which rely on similarity theory, the direct covariance method provides a direct computation of the wind stress. However, this method is highly susceptible to flow distortion and platform motion and is, therefore, difficult to implement in over-ocean studies. It is therefore preferable to develop indirect methods such as the bulk aerodynamic and inertial dissipation methods which relate easily measured quantities such as wind speed and temperature to the momentum flux. These methods allow us to estimate turbulent quantities when direct measurements are unavailable and to estimate the lower boundary flux conditions to input into numerical models.

The indirect methods for estimating momentum exchange rely on Monin-Obukhov similarity theory, which was developed almost half a century ago and has been validated over land by a number of field experiments. Its applicability over the ocean has only recently been examined. By quantitatively comparing the bulk and inertial dissipation

estimates to direct measurements, it was determined that the indirect methods systematically underestimate the momentum flux into developing seas. It was hypothesized that incorporating sea state dependence into the parameterizations would improve the wind stress estimations computed from both methods.

For the inertial dissipation method, a new parameterization for the dimensionless dissipation rate that includes the effects of the surface waves and accounts for the non-zero flux of energy from the atmosphere to the ocean is proposed:

$$\phi_{\varepsilon_m} = \phi_\varepsilon \left(1 - \frac{30u_*}{C_p}(2kz)e^{-2kz} \right) \tag{6.1}$$

This parameterization was developed from an independent data set and has resulted in over a 33% reduction of the error associated with the inertial dissipation friction velocity estimates when compared to direct covariance measurements.

Two separate methods of incorporating sea state dependence into the bulk aerodynamic method were explored. The first parameterization is based on the ideas of Donelan *et al.* (1993) and involved the derivation of a sea surface roughness length normalized by rms wave height that is a log-linear function of wave age:

$$\frac{z_r}{\sigma} = 9.6 \times 10^{-4} \left[\frac{U_{10}}{C_p} \right]^{2.7} \tag{6.2}$$

This parameterization agrees well with the relationships presented by Smith *et al.* (1992) and Donelan *et al.* (1993).

The parameterization was used in the bulk aerodynamic method and slightly improves the friction velocity estimates, although the difference is not statistically significant. The results indicate, however, an inherent bias and systematic trend in

overestimating u_*. One limitation is the lack of data with young wave ages so that the power law cannot be resolved well in the lower limit. Another possibility is that the log-linear relationship is too simplistic; the data suggest that a curve, or at least two lines, would provide a more optimal fit.

The second approach to modifying the bulk aerodynamic method involved incorporating a sea state dependent Charnock's parameter into the roughness length calculation:

$$z_r = \alpha_c \frac{u_*^2}{g} \tag{6.3a}$$

where

$$\alpha_c = -4.05\times10^{-4}\left(\frac{C_p}{U_{10N}}\right) + 2.34\times10^{-2} \tag{6.3b}$$

for $\frac{C_p}{u_*} < 43$.

When compared to the direct covariance measurements, this new parameterization resulted in a 7% reduction in the error associated with bulk aerodynamic friction velocity estimates and considerably improved drag coefficient estimates. The results are tentative due to the limited wave-age span upon which the function is derived, and more research is needed to validate or improve the shape of the function, especially in both the upper and lower limits.

Finally, this research strongly supports the use of either the bulk aerodynamic or inertial dissipation methods to estimate momentum exchange over the ocean. Since widespread direct measurements are not practical, indirect methods such as the bulk and

inertial dissipation methods are invaluable. While future research will undoubtedly improve the accuracy of both methods, especially as we gain increased understanding of wind-wave coupling, the results obtained here indicate that the current bulk aerodynamic and inertial dissipation algorithms which already have widespread acceptance are, in fact, doing an adequate job of estimating the momentum flux. This investigation provides strong quantitative evidence that incorporating sea state dependence into both methods takes us one step closer and improves upon current momentum flux estimates.

REFERENCES

Anctil, F., M. A. Donelan, W. M. Drennan, and H. C. Graber, 1994: Eddy-correlation measurements of air-sea fluxes from a discus buoy. *Journal of Atmospheric and Oceanic Technology*, **11**, 1144-1150.

Barstow, S. F., G. Ueland, H. E. Krogstad, and B. A. Fossum, 1991: The wavescan second generation directional wave buoy. *IEEE Journal of Oceanic Engineering*, **16**, 254-266.

Baumgartner, M. F. and S. P. Anderson, 1997: *Acquisition, Description and Evaluation of Atmospheric Model Products for the Coastal Mixing and Optics Experiment.* Woods Hole Oceanographic Institute Technical Report, WHOI-97-02, 1-29.

Bradley, E. F., P. A. Coppin, and J. S. Godfrey, 1991: Measurements of sensible and latent heat flux in the western equatorial Pacific Ocean. *Journal of Geophysical Research*, **96**, 3375-3389.

Businger, J. A., 1973: Turbulent transfer in the atmospheric surface layer. *Workshop on Micrometeorology*, D. A. Haugen, Ed., American Meteorological Society, 67-100.

Businger, J. A., J. C. Wyngaard, Y. Izumi, and E. F. Bradley, 1971: Flux-profile relationships in the atmospheric surface layer. *Journal of the Atmospheric Sciences*, **28**, 181-189.

Charnock, H., 1955: Wind stress on a water surface. *Quarterly Journal of the Royal Meteorological Society*, **81**, 639.

Davidson, K. L., C. E. Skupniewicz, D. Ross, R. G. Onstott, J. A. Johannessen, and O. Skagseth, 1991: Relationship between wind stress, backscatter, and the directional wave spectrum (NORCSEX-88). *Proceedings of OCEANS '91*, Honolulu, HI, IEEE, 998-1005.

Dobson, F. W., S. D. Smith, and R. J. Anderson, 1994: Measuring the relationship between wind stress and sea state in the open ocean in the presence of swell. *Atmosphere-Ocean*, **32**, 237-256.

Donelan, M. A., 1982: The dependence of the aerodynamic drag coefficient on wave parameters. *Proceedings of the 1st International Conference on Meteorology and Air-Sea Interaction of the Coastal Zone*, the Hague, American Meteorological Society, 381-387.

Donelan, M. A., 1990: Air-sea interaction. In *The Sea* (eds. B. LeMéhauté and D. M. Hanes). Wiley-Interscience, New York, 239-292.

Donelan, M. A., J. Hamilton, and W. H. Hui, 1985: Directional spectra of wind-generated waves. *Phil. Trans. Roy. Soc. London A*, **315**, 509-562.

Donelan, M. A., F. W. Dobson, S. D. Smith, and R. J. Anderson, 1993: On the dependence of sea surface roughness on wave development. *Journal of Physical Oceanography*, **23**, 2143-2149.

Dugan, J. P., S. L. Panichas, and R. L. DiMarco, 1991: Decontamination of wind measurements from buoys subject to motions in a seaway. *Journal of Atmospheric and Oceanic Technology*, **8**, 85-95.

Dyer, A. J., 1974: A review of flux-profile relationships. *Boundary Layer Meteorology*, **7**, 363-372.

Dyer, A. J. and B. B. Hicks, 1982: Kolmogorov constants at the 1976 ITCE. *Boundary Layer Meteorology*, **22**, 137-150.

Earle, D. M. and J. M. Bishop, 1984: *A Practical Guide to Ocean Wave Measurement and Analysis*. ENDECO, Inc., Marion, MA, 78 pp.

Edson, J. B., C. W. Fairall, P. G. Mestayer, and S. E. Larsen, 1991: A study of the inertial-dissipation method for computing air-sea fluxes. *Journal of Geophysical Research*, **96**, 10689-10711.

Edson, J. B., S. Wetzel, C. Friehe, S. Miller, and T. Hristov, 1997: Energy flux and dissipation profiles in the marine surface layer. *Proceedings of the 12th Symposium on Boundary Layers and Turbulence*, Vancouver, BC, Canada, American Meteorological Society, 314-315.

Edson, J. B., A. A. Hinton, K. E. Prada, J. E. Hare, and C. W. Fairall, 1998: Direct covariance flux estimates from mobile platforms at sea. *Journal of Atmospheric and Oceanic Technology*, **15**, 547-562.

Edson, J. B. and C. W. Fairall, 1998: Similarity relationships in the marine atmospheric surface layer for terms in the TKE and scalar variance budgets. *Journal of the Atmospheric Sciences*, **55**, 2311-2328.

Fairall, C. W. and S. E. Larsen, 1986: Inertial-dissipation methods and turbulent fluxes at the air-ocean interface. *Boundary Layer Meteorology*, **34**, 287-301.

Fairall, C. W., J. B. Edson, S. E. Larsen, and P. G. Mestayer, 1990: Inertial-dissipation air-sea flux measurements: a prototype system using realtime spectral computations. *Journal of Atmospheric and Oceanic Technology*, **7**, 425-453.

Fairall, C. W., E. F. Bradley, D. P. Rogers, J. B. Edson, and G. S. Young, 1996a: Bulk parameterization of air-sea fluxes for Tropical Ocean-Global Atmosphere Coupled-Ocean Atmosphere Response Experiment. *Journal of Geophysical Research*, **101**, 3747-3764.

Fairall, C. W., E. F. Bradley, J. S. Godfrey, G. A. Wick, J. B. Edson, and G. S. Young, 1996b: Cool-skin and warm-layer effects on sea surface temperature. *Journal of Geophysical Research*, **101**, 1295-1308.

Fairall, C. W., A. B. White, J. B. Edson, and J. E. Hare, 1997: Integrated shipboard measurements of the marine boundary layer. *Journal of Atmospheric and Oceanic Technology*, **14**, 338-359.

Finnigan, J. J., F. Einuadi, and D. Fua, 1984: The interaction between an internal gravity wave and turbulence in the stably-stratified nocturnal boundary layer. *Journal of Atmospheric Sciences*, **41**, 2409-2436.

Frederickson, P. A., K. L. Davidson, and J. B. Edson, 1997: A study of wind stress determination methods from a ship and an offshore tower. *Journal of Atmospheric and Oceanic Technology*, **14**, 822-834.

Frenzen, P. and C. A. Vogel, 1992: The turbulent kinetic energy budget in the atmospheric surface layer: a review and an experimental reexamination in the field. *Boundary Layer Meteorology*, **60**, 49-76.

Fujitani, T., 1981: Direct measurement of turbulent fluxes over the sea during AMTEX. *Papers in Meteorology and Geophysics*, **32**, 119-134.

Fujitani, T., 1985: Method of turbulent flux measurement on a ship by using a stable platform system. *Papers in Meteorology and Geophysics*, **36**, 157-170.

Galbraith, N., W. Ostrom, B. Way, S. Lentz, S. Anderson, M. Baumgartner, A. Plueddemann, and J. Edson, 1997: *Coastal Mixing and Optics Experiment: Mooring Deployment Cruise Report*. Woods Hole Oceanographic Institute Technical Report, WHOI-97-13, 81 pp.

Garratt, J. R., 1992: *The Atmospheric Boundary Layer*. Cambridge University Press, New York, 316 pp.

Geernaert, G. L., 1990: Bulk parameterizations for the wind stress and heat fluxes. In *Surface Waves and Fluxes, Volume I* (eds. G. L. Geernaert and W. J. Plant). Kluwer Academic Publishers, Boston, 91-172.

Geernaert, G. L., K. B. Katsaros, and K. Richter, 1986: Variation of the drag coefficient and its dependence on sea state. *Journal of Geophysical Research*, **91**, 7667-7679.

Geernaert, G. L., S. E. Larsen, and F. Hansen, 1987: Measurements of the wind stress, heat flux, and turbulence intensity during storm conditions over the North Sea. *Journal of Geophysical Research*, **92**, 13127-13139.

Geernaert, G. L., K. L. Davidson, S. E. Larsen, and T. Mikkelsen, 1988: Wind stress measurements during the Tower Ocean Wave and Radar Dependence Experiment. *Journal of Geophysical Research*, **93**, 13913-13923.

Gill, A. E., 1982: *Atmosphere-Ocean Dynamics*. Academic Press, San Diego, 662 pp.

Hare, J. E., J. B. Edson, E. J. Bock, and C. W. Fairall, 1992: Progress on direct covariance measurements of air-sea fluxes from ships and buoys. *Tenth Symposium on Turbulence and Diffusion*, Portland, OR, American Meteorological Society, 281-284.

Henjes, K., P. K. Taylor, and M. J. Yelland, 1998: Effect of pulse averaging on sonic anemometer spectra. *Journal of Atmospheric and Oceanic Technology*, in press.

Hicks, B. B., 1978: Some limitations of dimensional analysis and power laws. *Boundary-Layer Meteorology*, **14**, 567-569.

Hicks, B. B. and A. J. Dyer, 1972: The spectral density technique for determination of eddy fluxes. *Quarterly Journal of the Royal Meteorological Society*, **98**, 838-844.

Hill, R. J., 1996: Corrections to Taylor's frozen turbulence approximation. *Atmospheric Research*, **40**, 153-175.

Högström, U., 1987: Non-dimensional wind and temperature profiles in the atmospheric surface layer: a re-evaluation. *Boundary Layer Meteorology*, **42**, 55-78.

Högström, U., 1996: Review of some basic characteristics of the atmospheric surface layer. *Boundary Layer Meteorology*, **78**, 215-246.

Janssen, P. A. E. M., 1989: Wave-induced stress and the drag of air flow over sea waves. *Journal of Physical Oceanography*, **19**, 745-754.

Kaimal, J. C., J. C. Wyngaard, and D. A. Haugen, 1968: Deriving power spectra from a three-component sonic anemometer. *Journal of Applied Meteorology*, **7**, 827-837.

Kitaigorodskii, S. A., 1973: *The Physics of Air-Sea Interaction*, translated from Russian, Israel Program for Scientific Translations, Jerusalem, 237 pp.

Large, W. G. and J. A. Businger, 1988: A system for remote measurements of the wind stress over the ocean. *Journal of Atmospheric and Oceanic Technology*, **5**, 274-285.

Large, W. G. and S. Pond, 1981: Open ocean momentum flux measurements of the wind stress over the ocean. *Journal of Physical Oceanography*, **11**, 324-336.

Lumley, J. L. and H. A. Panofsky, 1964: *The Structure of Atmospheric Turbulence*. J. Wiley and Sons, New York, 229 pp.

Maat, N., C. Kraan, and W. A. Oost, 1991: The roughness of wind waves. *Boundary Layer Meteorology*, **54**, 89-103.

Mahrt, L., D. Vickers, J. Howell, J. Højstrup, M. Courtney, J. M. Wilczak, J. B. Edson, and J. Hare, 1996: Sea surface drag coefficients in Risø Air Sea Experiment (RASEX). *Journal of Geophysical Research*, **101**, 14327-14335.

Miller, M. J., A. C. M. Beljaars, and T. N. Palmer, 1992: The sensitivity of the ECMWF model to the parameterization of evaporation from the tropical oceans. *Journal of Climate*, **5**, 418-434.

Monin, A. S. and A. M. Obukhov, 1954: Basic laws of turbulent mixing in the surface layer of the atmosphere. *Trudy Geofizicheskogo Instituta Akademiya Nauk SSSR*, **24**,163-187.

Nordeng, T. E., 1991: On the wave age dependent drag coefficient and roughness length at sea. *Journal of Geophysical Research*, **96**, 7167-7174.

Panofsky, H. A. and J. A. Dutton, 1984: *Atmospheric Turbulence*. Wiley-Interscience, New York, 397 pp.

Shaw, W. J., 1990: Theory and scaling of lower atmospheric turbulence. In *Surface Waves and Fluxes, Volume I* (eds. G. L. Geernaert and W. J. Plant). Kluwer Academic Publishers, Boston, 63-72.

Smith, S. D., 1980: Wind stress and heat flux over the ocean in gale force winds. *Journal of Physical Oceanography*, **10**, 709-726.

Smith, S. D., 1988: Coefficients for sea surface wind stress, heat flux, and wind profiles as a function of wind speed and temperature. *Journal of Geophysical Research*, **93**, 15467-15472.

Smith, S.D., 1991: Some early results of the Humidity Exchange over the Sea main experiment. In *Deep Convection and Deep Water Formation in the Oceans* (eds. P. C. Chu and J. C. Gascard). Elsevier Science Publishers, Amsterdam, 377-382.

Smith, S.D., R. J. Anderson, W. A. Oost, C. Kraan, N. Maat, J. DeCosmo, K. B. Katsaros, K. L. Davidson, K. Bumke, L. Hasse, and H. M. Chadwick, 1992: Sea surface wind stress and drag coefficients: The HEXOS results. *Boundary Layer Meteorology*, **60**, 109-142.

Smith, S. D., C. W. Fairall, G. L. Geernaert, and L. Hasse, 1996: Air-sea fluxes: 25 years of progress. *Boundary Layer Meteorology*, **78**, 247-290.

Stenner, R., 1996: Coastal Mixing and Optics Experimental Site (http://wavelet.apl.washington.edu/CMO/CMO_bath.html).

Thiermann, V. and H. Grassl, 1992: The Measurement of turbulent surface layer fluxes by use of Bichromatic Scintillation. *Boundary Layer Meteorology*, **58**, 367-389.

Tsukamoto, O., E. Ohtaki, H. Ishida, M. Horiguchi, and Y. Mitsuta, 1990: On-board direct measurements of turbulent fluxes over the open sea. *Journal of the Meteorological Society of Japan*, **68**, 203-211.

Vogel, C. A. and P. Frenzen, 1992: A new study of the TKE budget in the surface layer, Part II: The dimensionless function and divergent transport terms. *Proceedings of the 10th Symposium on Turbulence and Diffusion*, Portland, OR, American Meteorological Society, 161-164.

Wallace, J. M. and P. V. Hobbs, 1977: *Atmospheric Science*. Academic Press, San Diego, 467 pp.

Webb, E. K., G. I. Pearman, and R. Leuning, 1980: Correction of flux measurements for density effects due to heat and water vapor transport. *Quarterly Journal of the Royal Meteorological Society*, **106**, 85-100.

Webster, P. J. and R. Lukas, 1992: TOGA COARE: The Coupled Ocean Atmosphere Response Experiment. *Bulletin American Meteorological Society*, **73**, 1377-1416.

Weller, R. A., D. L. Rudnick, R. E. Payne, J. P. Dean, N. J. Pennington, and R. P. Trask, 1990: Measuring near-surface meteorology over the ocean from an array of surface moorings in the subtropical convergence zone. *Journal of Atmospheric and Oceanic Technology*, **7**, 85-103.

Williams III, A. J., 1997: Introduction. *Coastal Mixing and Optics Report III, Proceedings of the Coastal Mixing and Optics Meeting*, Santa Fe, NM, 139 pp.

Wu, J., 1980: Wind-stress coefficients over sea surface near neutral conditions—a revisit. *Journal of Physical Oceanography*, **10**, 727-740.

Wyngaard, J. C., 1973: On surface layer turbulence. *Workshop on Micrometeorology*, D. A. Haugen, Ed., American Meteorological Society, 101-149.

Wyngaard, J. C. and S. F. Clifford, 1977: Taylor's Hypothesis and high frequency turbulence spectra. *Journal of the Atmospheric Sciences*, **34**, 922-928.

Yelland, M. J., P. K. Taylor, I. E. Consterdine, and M. H. Smith, 1994: The use of the inertial dissipation technique for shipboard wind stress determination. *Journal of Atmospheric and Oceanic Technology*, **11**, 1093-1108.

Yelland, M. J. and P. K. Taylor, 1996: Wind stress measurements from the open ocean. *Journal of Physical Oceanography*, **26**, 541-558.